2

Solid State Research

1971

Prepared under Electronic Systems Division Contract F19628-70-C-0230 by

Lincoln Laboratory

MASSACHUSETTS INSTITUTE OF TECHNOLOGY

Lexington, Massachusetts

Approved for public release; distribution unlimited.

2

Solid State Research

1971

Issued 9 August 1971

Prepared under Electronic Systems Division Contract F19628-70-C-0230 by

Lincoln Laboratory

MASSACHUSETTS INSTITUTE OF TECHNOLOGY

Lexington, Massachusetts

The work reported in this document was performed at Lincoln Laboratory, a center for research operated by Massachusetts Institute of Technology, with the support of the Department of the Air Force under Contract F19628-70-C-0230.

ABSTRACT

This report covers in detail the solid state research work of the Solid State Division at Lincoln Laboratory for the period 1 February through 30 April 1971. The topics covered are Solid State Device Research, Materials Research, Physics of Solids and Microelectronics. The Microsound work is sponsored by ABMDA and is reported under that program.

Accepted for the Air Force
Joseph R. Waterman, Lt. Col., USAF
Chief, Lincoln Laboratory Project Office

INTRODUCTION

1. SOLID STATE DEVICE RESEARCH

Progress has been made in improving the performance of InSb photodiodes and photodiode arrays fabricated by proton bombardment. Through the development of new surface coating and passivating techniques, the 77°K reduced background peak detectivities of these photodiodes at 4.8 μm have been increased from 3 to 5 × 10^{11} cmHz$^{1/2}$/W to 1.1 × 10^{12} cmHz$^{1/2}$/W. In addition, planar, uniform, multielement arrays of InSb photodiodes have been fabricated in which all elements are high sensitivity active devices.

CW, tunable, diode lasers of $PbS_{1-x}Se_x$ have been fabricated with output in the wavelength region near 5 μm. The variation of emission wavelength with composition, temperature, magnetic field and current through the diode was obtained. CW power of 8 μW at 12°K from a tunable $PbS_{0.82}Se_{0.18}$ diode laser emitting at 4.74 μm with an estimated linewidth of 1 MHz was measured at one end of the cavity. The doppler linewidth and doppler limited absorption coefficient at room temperature of the P(9) fundamental absorption line of CO at 2107.4 cm^{-1} were determined by tuning the laser line with current through the absorption line.

Preliminary results have been obtained on the epitaxial growth of $In_xGa_{1-x}As$ alloys of low indium composition using an In-Ga-$AsCl_3$-H_2 open tube flow system. Single crystal n-type alloy layers 41 to 83 μm thick were obtained with energy gaps between 1.28 and 1.25 eV (vs 1.41 for GaAs), carrier concentrations between 1.4 and 9.2 × 10^{14} cm^{-3} and room temperature mobilities between 5500 and 7100 cm^2/V-sec. Mobilities at 77°K as high as 72,000 cm^2/V-sec have been obtained.

GaAs Schottky barrier mixer diodes suitable for 50 GHz mixers have been fabricated using a technique designed to minimize parasitic parallel capacitances, series resistance and series inductance. The fabrication is accomplished in two distinct series of steps dealing with the two sides of a GaAs layer, and results in active devices formed on pockets of GaAs about 2 μm thick and 1 by 3 mils in area. Measurements made at low frequencies indicate that the diodes have zero-bias capacitances of 0.02 to 0.03 pF and impedances of 30 to 50 ohms.

Acoustic surface wave delay lines of 270 MHz with 5 MHz bandwidth and delay of 1.8 μsec have been fabricated on (100) surface semi-insulating GaAs (aligned along the [011] axis). Using double stub tuners the insertion loss was reduced to 15 dB, most of which was due to the electrical mismatch between the 50-ohm RF generator and the 5-ohm impedance of the transducers. Measurements on longer (3.6 μsec) delay lines indicate that the propagation losses for this cut of GaAs are less than 0.5 dB/μsec at 270 MHz.

A program has been undertaken to develop a process utilizing x-radiation to replicate extremely high resolution microelectronic patterns. These submicron structures will be written with a scanning electron microscope into specially designed x-ray pattern masks. Such patterns can then be reproduced an unlimited number of times since the large spacing between the mask and wafer, allowable with x-rays, greatly reduces the chance of damage to the pattern mask.

II. MATERIALS RESEARCH

The insulating properties of embossed tantalum sheet (in the form of multiple heat shields) and stabilized zirconia felt have been tested up to 2550° and 2300°C, respectively. These are promising materials for use in insulating high temperature furnaces because of the convenience with which they can be fabricated into the required forms.

A new compound with perovskite structure, $BiRhO_3$, has been prepared by high-pressure synthesis. The compound is formed when a stoichiometric mixture of Bi_2O_3 and Rh_2O_3 is placed in a platinum capsule and subjected to a pressure of over 65 kbar at 1000° to 1300°C for one-half hour.

Whereas VO_2 has a single monoclinic-to-tetragonal phase transformation at a semiconductor-to-metal transition, several $V_{1-x}M_xO_2$ systems exhibit two crystallographic changes: monoclinic-to-orthorhombic at T_t' and orthorhombic-to-tetragonal at T_t. We point out that there are two components to the deformation to monoclinic symmetry: an antiferroelectric displacement of the cations and the formation of V-V homopolar-bonded pairs. Changes in T_t and T_t' with x and the cation M can be accounted for by a model of the orthorhombic phase as a deformation induced primarily by antiferroelectric displacements. A structure refinement of orthorhombic $V_{0.95}Cr_{0.05}O_2$ shows that one-half of the V ions exhibit purely antiferroelectric displacements, one-quarter purely V-V bonding, and the remaining quarter remain in the center of symmetry of a distorted interstice as in a Jahn-Teller distortion.

Single crystals of semiconducting ferromagnetic $Fe_{1-x}Cu_xCr_2S_4$ alloys up to 5 mm on a side have been grown by a closed-tube vapor transport technique which uses $CrCl_3$ as the transport agent. When the crystals are annealed in vacuum or in sulfur vapor, their lattice parameters are significantly affected by the resulting changes in the sulfur-to-metal ratio.

The effects of hydrostatic pressure on the electrical properties of n-type CdTe heavily doped with Cl, Br, Ga, or In show that the effective donor levels introduced by these impurities are associated primarily with a conduction band minimum lying above the lowest minimum at $\Gamma(k = 0)$. The transfer of electrons between these non-Γ levels and the Γ minimum is a thermally activated process which at sufficiently low temperatures becomes too slow for equilibrium to be achieved experimentally.

III. PHYSICS OF SOLIDS

Extension of Shubnikov-de Haas measurements in $Pb_{1-x}Sn_xSe$ ($x = 0.17$ and 0.20) to high magnetic fields has allowed the observation of spin splitting. Large and isotropic g-factors ($87 \geqslant g \geqslant 48$), which depend on doping, are determined from these measurements.

Experimental measurements have been carried out for the voltage dependence of the incremental capacitance of evaporated metal Schottky barriers on p-InAs and p-PbTe. The results have been interpreted in terms of a theory which takes the inverted surface layer into account and which holds even when the band bending in the semiconductor exceeds the energy gap.

Preliminary studies of optically pumped stimulated emission from homogeneous n-PbTe platelets have been carried out, using a Q-switched CO gas laser as a pump. Although the conversion efficiency in these experiments is low (<1 percent), this system holds two promising possibilities, namely: resonant pumping near the PbTe energy gap, and stimulated spin-flip scattering.

Work on the identification of the intense 1082 cm^{-1} line in FeF_2, previously observed by Raman scattering, has been augmented by infrared absorption measurements as well as Raman scattering of MnF_2 and MgF_2 doped with Fe^{2+}. Present evidence suggests that this line is either (a) a pair-excitation involving a crystal field state and a magnon or (b) a single ion excitation involving the exchange field and spin-orbit coupling.

A finite temperature, two-magnon Raman scattering theory, developed to describe observations in a three-dimensional antiferromagnet, has been extended to the description of the two-dimensional antiferromagnet K_2NiF_4. The results should contain information on the persistence of short-range order above the critical temperature for the disappearance of long range order.

A study has been carried out of a permanent (at least 3 days) lens effect induced by illumination with a low power 6328 Å laser in bulk samples of high-conductivity single crystal CdS at temperatures above 100°C. The lens is erasable by annealing at higher temperatures.

IV. MICROELECTRONICS

Several service-oriented programs have made notable progress in the past quarter as evidenced by the operating performance obtained on E-Birds, TRAPATT and gallium arsenide devices. Characteristically, however, these developmental programs are often open ended in terms of secondary specifications such as power handling capabilities, minimum noise figure and physical configuration. As a result, new phases of development often follow the initial phase of work in order to achieve greater levels of circuit performance. The degree of success achieved in these secondary program phases is based on further process refinements, control of process parameters and the over-all integration of masks, materials, processing, assembly and packaging techniques, and is limited by the uncertainties inherent in any developmental program. In those cases where similar commercial work is available for comparison, the devices fabricated here exhibit better characteristics and the over-all development time is shorter although considerably longer than we would like.

Several developmental programs related to interconnections, assembly and fabrication, particularly the beam leaded substrates, gridded ceramic substrates and the SIMTOP process are being adopted in commercial as well as internal programs.

The development of the laser scanner for testing devices and monolithic integrated circuits is continuing. The usefulness of the system for diagnostic purposes and the testing of multichip assemblies has been established. The limitations of the system in testing MOS (metal oxide silicon) structures and LSI (large-scale integration) are currently being evaluated in terms of the defects and faults that can be seen and the problems associated with computerizing the output data.

CONTENTS

REPORTS ON SOLID STATE RESEARCH

15 February through 15 May 1971

PUBLISHED REPORTS

Journal Articles*

JA No.			
3684	Growth of EuO, EuS, EuSe and EuTe Single Crystals	T.B. Reed R.E. Fahey	J. Crystal Growth 8, 337 (1971)
3747	Electron Spin Waves in Nonmagnetic Conductors: Self-Consistent-Field Theory	F.A. Blum	Phys. Rev. B 3, 2258 (1971)
3748	Shubnikov-de Haas Measurements in $Pb_{1-x}Sn_xTe$	J. Melngailis T.C. Harman J.G. Mavroides J.O. Dimmock	Phys. Rev. B 3, 370 (1971) DDC AD-721065
3758	Critical Magnetic Properties and Exchange Interactions in EuO	N. Menyuk K. Dwight T.B. Reed	Phys. Rev. B 3, 1689 (1971)
3761	Conceptual Phase Diagram and Its Application to the Spontaneous Magnetism of Several Pyrites	J.B. Goodenough	J. Solid State Chem. 3, 26 (1971)
3782	Type Conversion and n-p Junction Formation in $Hg_{1-x}Cd_xTe$ Produced by Proton Bombardment	A.G. Foyt T.C. Harman J.P. Donnelly	Appl. Phys. Letters 18, 321 (1971)
3785	Rapid Scanning Microscope for Light Probing and Infrared Mapping	R.J. Phelan, Jr.† N.L. DeMeo, Jr.	Appl. Opt. 10, 858 (1971)
3788	Field-Dependent Central-Cell Corrections in GaAs by Laser Spectroscopy	H.R. Fetterman D.M. Larsen G.E. Stillman P.E. Tannenwald J. Waldman†	Phys. Rev. Letters 26, 975 (1971)
3795	The Fermi Surface and Optical Properties of Potassium	G. Dresselhaus A.R. Wilson C-Y. Young	Solid State Commun. 8, 2125 (1970)

* Reprints available.

† Author not at Lincoln Laboratory.

Reports

JA No.			
3804	Effects of Short-Range Interactions on Electron-Charge Ordering and Lattice Distortions in the Localized State	R. A. Bari	Phys. Rev. B 3, 2662 (1971)
3812	Two-Magnon Raman Scattering and Exchange Interactions in Antiferromagnetic $KNiF_3$ and K_2NiF_4 and Ferrimagnetic $RbNiF_3$	S. R. Chinn H. J. Zeiger J. R. O'Connor	Phys. Rev. B 3, 1709 (1971)
3813	n-p Junction Photovoltaic Detectors in PbTe Produced by Proton Bombardment	J. P. Donnelly T. C. Harman A. G. Foyt	Appl. Phys. Letters 18, 259 (1971)
3831	Anomalously High "Mobility" in Semiconductors	C. M. Wolfe G. E. Stillman	Appl. Phys. Letters 18, 205 (1971)
3850	Efficient, Single-Mode, cw, Tunable Spin-Flip Raman Laser	S. R. J. Brueck A. Mooradian	Appl. Phys. Letters 18, 229 (1971)
3854	Laser Tests ICs with Light Touch	R. E. McMahon	Electronics 44, 92 (1971)
3857	Observation of Nonextremal Fermi-Surface Orbits in Bulk Bismuth	V. E. Henrich	Phys. Rev. Letters 26, 891 (1971)
MS No.			
2891	Optical Properties of the Alkalis Using the KKR-Z Method	A. Wilson G. Dresselhaus C-Y. Young	Computational Methods in Band Theory, edited by P. M. Marcus, J. F. Janak and A. R. Williams (Plenum Press, New York, 1971); Proceedings Conference on Computational Methods in Band Theory, Yorktown Heights, New York, 14-15 May 1970
2951	Localized versus Itinerant Electrons in Magnetic Solids	J. B. Goodenough	Summer School on the Theory of Magnetism of Metals, Zakopane, Poland, 31 August – 11 September 1970, Vol. 1 (Institute of Physics of the Polish Academy of Sciences, 1971), pp. 124-329
2959	Magnetic Properties of Europium: Pressure and Impurity Effects	N. Menyuk K. Dwight J. A. Kafalas	J. Appl. Phys. 42, 1301 (1971)
2961	Effect of Pressure on the Magnetic Properties of $Ca_{1-x}Sr_xMnO_3$	J. A. Kafalas N. Menyuk K. Dwight J. M. Longo	J. Appl. Phys. 42, 1497 (1971)

MS No.			
2966	High Pressure $RbFeCl_3$ – A Transparent Ferrimagnet	J. M. Longo J. A. Kafalas N. Menyuk K. Dwight	J. Appl. Phys. 42, 1561 (1971)
2970	Magnetic Phase Transitions in EuTe	N. F. Oliveira, Jr.* S. Foner* Y. Shapira* T. B. Reed	J. Appl. Phys. 42, 1783 (1971)

* * * * *

UNPUBLISHED REPORTS

Journal Articles

JA No.			
3752A	A Raman Study of the Semiconductor-Metal Transition in Ti_2O_3	A. Mooradian P. M. Raccah	Accepted by Phys. Rev. B
3791	Theory of Electron-Surface Plasmon Interactions in Tunneling, Low Energy Electron Diffraction and in Photoemission	K. L. Ngai E. N. Economou*	Accepted by Phys. Rev. B
3838	Far Infrared Mixing in High-Purity GaAs	B. Y. Lao M. M. Litvak	Accepted by J. Appl. Phys.
3847	Carrier Concentration and Mobility in n- and p-Type ZnTe-Al	F. T. J. Smith	Accepted by Solid State Commun.
3863	Raman Spectra and Lattice Dynamics of Tellurium	A. S. Pine G. Dresselhaus	Accepted by Phys. Rev. B
3867	Spin Wave Approach to Two-Magnon Raman Scattering in a Simple Antiferromagnet	R. W. Davies S. R. Chinn H. J. Zeiger	Accepted by Phys. Rev.
3868	The Two Components of the Crystallographic Transition in VO_2	J. B. Goodenough	Accepted by J. Solid State Chem.
3887	High Pressure Synthesis of $(ABX_3)(AX)_n$ Compounds	J. A. Kafalas J. M. Longo	Accepted by J. Solid State Chem.

* Author not at Lincoln Laboratory.

Meeting Speeches*

MS No.			
2757A	Metal-Semiconductor Contacts on $Pb_{1-x}Sn_xTe$	K. W. Nill	Seminar, U. S. Naval Ordnance Laboratory, White Oak, Silver Spring, Maryland, 15 April 1971
2799C	Optical Study of the Semiconductor to Metal Transition in Ti_2O_3	P. M. Raccah	Seminar, New York University, 23 February 1971
2989A	Testing Integrated Circuits with a Laser Beam	R. E. McMahon	XVIII Congresso Scientifico Internazionale Per L'Electronica, Rome, Italy, 29-31 March 1971
3001	High Apparent Mobility in Inhomogeneous Semiconductors	C. M. Wolfe G. E. Stillman J. A. Rossi	139th National Meeting, The Electrochemical Society, Washington, D.C., 9-14 May 1971
3008	A Comparative Study of Liquid Solution Models for III-V and II-VI Binary Systems	J. M. Steininger R. F. Brebrick	
3122	Crystal Growth and Properties of Semiconducting, Ferromagnetic $Fe_{1-x}Cu_xCr_2S_4$ Alloys	M. D. Banus A. J. Strauss	
3026	Transparent Gold Films for High Temperature Furnaces	T. B. Reed W. J. LaFleur	73rd Annual Meeting, American Ceramic Society, Chicago, 24-29 April 1971
3027	Multilayer Interconnections on Ceramic	F. J. Bachner H. H. Pichler	
3065	Semiconductor-to-Metal Transition in VO_2	J. B. Goodenough	
3032	Polaron Self-Energy Effects on Higher Landau Levels in InSb	E. J. Johnson K. L. Ngai	American Physical Society Meeting, Cleveland, 29 March – 1 April 1971
3042	Non-extremal Fermi Surface Areas in Bismuth	V. E. Henrich	
3045	Optical Study of Spin-Flop in Cr_2O_3	J. W. Allen	
3046	Phonon Dispersion Relations in Tellurium	G. Dresselhaus A. S. Pine	
3047	Galvanomagnetic Measurements at Hydrostatic Pressure on $Hg_{1-x}Cd_xTe$ Alloys Near the Semimetal-Semiconductor Transition	C. T. Elliott J. Melngailis T. C. Harman J. A. Kafalas	
3048	Shubnikov-de Haas Measurements in $Pb_{1-x}Sn_xSe$	J. Melngailis T. C. Harman	

* Titles of Meeting Speeches are listed for information only. No copies are available for distribution.

MS No.			
3049	Capacitance-Voltage Measurements on lnAs and PbTe Schottky Barriers: Effects of the lnverted Surfaces	K. W. Nill J. N. Walpole*	
3050	Calorimetry, Normal Incidence Optical Spectra and Magnetic Properties of the $NiS_{(1-x)}Se_x$ System Across the Semiconductor-to-Metallic Transition	P. M. Raccah J. B. Goodenough	
3051	Absolute Experimental X-Ray Form Factor of Copper	R. J. Temkin V. E. Henrich P. M. Raccah	
3056	Lattice and Correlation Effects on Narrow-Band Electrons	R. A. Bari	
3057	How Hydrogenic are Shallow Donors in GaAs?	R. C. Brandt G. E. Stillman D. M. Larsen C. M. Wolfe	American Physical Society Meeting, Cleveland, 29 March – 1 April 1971
3058	Efficient, Single Mode, CW, Tunable Spin-Flip Raman Laser	S. R. J. Brueck A. Mooradian	
3059	Effect of Hydrostatic Pressure on Electrical Porperties of n-Type CdTe	G. W. lseler J. A. Kafalas A. J. Strauss	
3061	Multielectron Field Emission	K. L. Ngai R. A. Bari	
3062	lnterband Magnetoreflection of $Hg_xCd_{1-x}Te$	C. R. Pidgeon* T. C. Harman S. H. Groves	
3063	Kinetics of Electron Transfer in n-Type CdTe	A. J. Strauss G. W. lseler J. A. Kafalas	
3066	Lineshapes of Spontaneous Spin-Flip Light Scattering in Semiconductors	F. A. Blum S. R. J. Brueck	
3043B, 3043C, 3043D	Semiconductor-to-Metal Transitions	J. B. Goodenough	Colloquium, The University of Manitoba, Winnipeg, Canada, 9 March 1971; Solid State Seminar, University of California, Berkeley, 10 March 1971; Solid State Science and Engineering Colloquia, Columbia University, 24 March 1971

* Author not at Lincoln Laboratory.

Reports

MS No.			
3051A	Absolute Experimental X-Ray Form Factor of Copper	R. J. Temkin	Solid State Physics Seminar, Purdue University, 19 April 1971
3060A	Laser Magneto-Spectroscopy of Field Dependent Central Cell Corrections in GaAs Donors	H. R. Fetterman D. M. Larsen J. Waldman*	American Physical Society Meeting, Washington, D.C., 26-29 April 1971
3082	Acoustical Activity and Shear Wave Dispersion in Quartz	A. S. Pine	
3086	Magnetic Phase Transition and Self-Consistent Magnetic Induction in Itinerant Antiferromagnetism	C-Y. Young J. W. Allen	
3093	Paramagnetic Resonance in Ferrous Fluosilicate at Sub-millimeter Wavelengths	R. S. Rubins* H. R. Fetterman	
3067	Polaron Morphologies in Vanadium Oxides	J. B. Goodenough	International Conference on Conduction in Low Mobility Materials, Eilat, Israel, 5-8 April 1971
3077	Type Conversion and N-P Junction Formation in $Hg_{1-x}Cd_xTe$ Produced by Proton Bombardment	A. G. Foyt T. C. Harman J. P. Donnelly	IRIS Detector Specialty Group Meeting, San Diego, 17-18 March 1971
3078	N-P Junction Photovoltaic Detectors in PbTe and $Pb_{1-x}Sn_xTe$ Produced by Proton Bombardment	J. P. Donnelly T. C. Harman A. G. Foyt	
3079	Development of N-P Junction Photovoltaic Detectors in InSb Fabricated Using Proton Bombardment	A. G. Foyt W. T. Lindley J. P. Donnelly	
3080	High Speed $Hg_{1-x}Cd_xTe$ Photodiodes	I. Melngailis T. C. Harman E. D. Hinkley W. T. Lindley	
3091A, 3091B	Optical Properties of the Alkalis Using the KKR-Z Method	C-Y. Young	Physics Seminar, Northeastern University, 3 March 1971; University of Massachusetts, Boston, 9 April 1971
3095, 3095A	Lattice Distortions and Mott Insulators	R. A. Bari	Physics Seminar, Northeastern University, 24 February 1971; New York University, 1 March 1971

* Author not at Lincoln Laboratory.

MS No.			
3102	Some Comparisons of Oxides and Fluorides of the Transition Elements	J. B. Goodenough	Conference on New Fluorides and Their Physical Properties, Montpellier, France, 2 April 1971
3106	Empirical Regularities in Exchange Processes	J. B. Goodenough	Conference on Exchange Interactions Between Ions in Crystals and Molecules, Princeton University, 12-14 May 1971
3112	Stimulated and Spontaneous Spin-Flip Raman Scattering in InSb	S. R. J. Brueck	Seminar, M.I.T., 22 March 1971
3123	Introduction to Nonlinear Optics	P. L. Kelley	Spring Meeting, New England Section, American Physical Society, Amherst College, 2-3 April 1971
3133	Lattice Dynamics and Light Scattering in Optically Active Crystals	G. Dresselhaus	Physics Seminar, Purdue University, 23 April 1971
3134	Infrared Photodiodes Fabricated by Proton Bombardment	J. O. Dimmock A. G. Foyt J. P. Donnelly T. C. Harman W. T. Lindley	11th Midcourse Measurements Meeting, San Bernardino, California, 20 April 1971

ORGANIZATION

SOLID STATE DIVISION

A. L. McWhorter, *Head*
P. E. Tannenwald, *Associate Head*
C. R. Grant, *Assistant*

OPTICAL AND ELECTRONIC PHYSICS

H. J. Zeiger, *Leader*
A. Mooradian, *Associate Leader*
P. L. Kelley, *Assistant Leader*

Bari, R. A.
Brodersen, R. W.*
Brueck, S. R. J.*
Burke, J. W.
Chinn, S. R.
Davies, R. W.
Dresselhaus, G. F.
Johnson, E. J.
Landon, S. N.
Larsen, D. M.
Ngai, K. L.
Palm, B. J.†
Pine, A. S.
Rossi, J. A.
Young, C-Y.

SOLID STATE PHYSICS

J. G. Mavroides, *Leader*
G. B. Wright, *Assistant Leader*

Allen, J. W.
Barch, W. E.
Blum, F. A., Jr.
DeFeo, W. E.
Dresselhaus, M. S.†
Dwight, K., Jr.
Feldman, B.
Fetterman, H.
Groves, S. H. (LOA)
Henrich, V. E.
Kernan, W. C.
Kolesar, D. F.
Melngailis, J.
Menyuk, N.
Nill, K. W.
Parker, C. D.

ELECTRONIC MATERIALS

J. B. Goodenough, *Leader*
A. J. Strauss, *Associate Leader*

Anderson, C. H., Jr.
Banus, M. D.
Batson, D. A.
Button, M. J.
Coppola, A. J.
Delaney, E. J.
Fahey, R. E.
Finn, M. C.
Iseler, G. W.
Kafalas, J. A.
LaFleur, W. J.
Lavine, M. C.†
Mastromattei, E. L.
Mroczkowski, I. H.
Owens, E. B.
Pantano, J. W.
Pierce, J. W.
Plonko, M. C.
Raccah, P. M.
Reed, T. B.
Temkin, R. J.*
Tracy, D. M.

APPLIED PHYSICS

J. O. Dimmock, *Leader*
T. C. Harman, *Assistant Leader*
I. Melngailis, *Assistant Leader*

Belanger, L. J.
Calawa, A. R.
Carter, F. B.
DeMeo, N.
Donnelly, J. P.
Elliott, C. T.‡
Ferrante, G. A.
Foyt, A. G.
Hancock, R. C.
Hurwitz, C. E.
Krohn, L., Jr.
Lindley, W. T.
McBride, W. F.
Murphy, R. A.*
Orphanos, W. G.
Paladino, A. E.
Spears, D. L.
Stillman, G. E.
Ward, J. H. R., III
Wolfe, C. M.
Woods, R. J.
Youtz, P.

MICROELECTRONICS

R. E. McMahon, *Leader*

Bachner, F. J.
Beatrice, P. A.
Childs, N. B.
Clough, T. F.
Cohen, R. A.
Durant, G. L.
Grant, L. L.
Gray, R. V.
McGonagle, W. H.
Mountain, R. W.
Pichler, H. H.
Pybus, V. J.
Wilde, R. E.

MICROSOUND

E. Stern, *Leader*

Alusow, J. A.
Brogan, W. T.
Burke, B. E.
Chen, F.
Smith, H. I.
Waldron, R. A.
Williamson, R. C.

---

* Research Assistant
† Part Time
‡ Visiting Scientist

I. SOLID STATE DEVICE RESEARCH

A. DEVELOPMENT OF N-P JUNCTION PHOTOVOLTAIC DETECTORS IN InSb FABRICATED USING PROTON BOMBARDMENT

In an earlier Solid State Research report,[1] we discussed our experiments on the use of proton bombardment to create n-type layers in p-type InSb, and the use of this technique in the fabrication of n-p junction photovoltaic detectors. Since that time, we have continued the development and evaluation of these devices. In this section, current evaluation data on a $1\frac{1}{2}$-year-old diode will be given. In addition, some array fabrication experiments and the use of a different surface coating to increase the zero-bias resistance of these diodes will be discussed.

The details of this fabrication technique are reviewed in Fig. I-1. The InSb substrate is p-type, with $p \sim 3 \times 10^{15}\ cm^{-3}$ at 77°K. Following a brief etch in 2:1:1 HNO_3:HAc:HF, the InSb is coated with a thin (1500 Å) layer of SiO_2 deposited at 340°C from a silane-oxygen reaction, and thin gold contacts are plated through 5-mil-diameter holes in the oxide. The sample is then covered with a thick layer of photoresist, and 20-mil-diameter holes are opened in the photoresist. This photoresist layer is sufficiently thick (~10 μm) to block the proton beam; consequently, only the InSb from which the photoresist has been removed is bombarded to create the n-type layer. Following the proton bombardment, the photoresist is removed and the diode is mounted in a liquid nitrogen dewar for electrical evaluation.

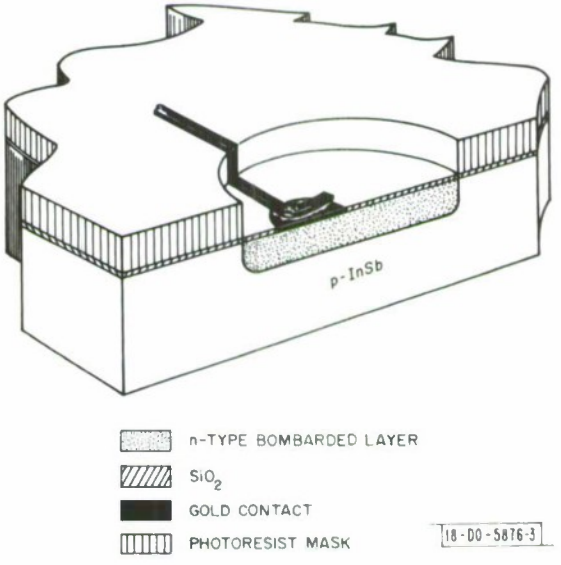

Fig. I-1. Sketch of a 20-mil-diameter InSb n-p junction diode, fabricated using proton bombardment to create the n-type layer.

The devices discussed previously had zero-bias resistances greater than 100 kohms at 77°K, and peak detectivities in excess of 10^{11} $cmHz^{1/2}/W$ at 4.8 μm. Also, it was shown that the diodes were unaffected by a three-month, 80°C life test.

Since the device shelf life is another important parameter, the diode characteristics were remeasured after $1\frac{1}{2}$ years in room ambient conditions. A comparison of device parameters is shown in Table I-1. The zero-bias capacitance of this diode has increased slightly, and the zero-bias resistance somewhat more dramatically. The quantum efficiency at the wavelength of peak response has not changed, but the detectivity in reduced background has increased as a result of the larger resistance. It should be noted that, in our recent measurements in reduced background, the measured device noise agrees with the thermal noise calculated for the diode resistance. In other words, no excess noise over thermal noise is measured in these diodes at 500 Hz, and the device detectivity is determined by its quantum efficiency and zero-bias resistance.

TABLE I-1

ROOM AMBIENT LIFE TEST DATA ON A 20-MIL-DIAMETER InSb n-p JUNCTION PHOTOVOLTAIC DETECTOR†

	November 1969	March 1971
C (0) [pF]	110	120
R (0) [megohm]	0.36	1.0
η (λ = 4.8 μm) [percent]	35	35
D^*_λ (4.8 μm) [cm $Hz^{1/2}/W$]	2×10^{11}	4×10^{11}

† Fabricated using proton bombardment to create the n-type layer.

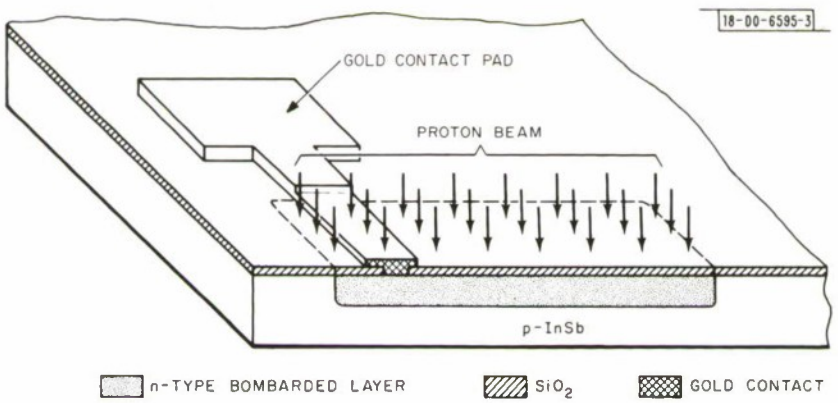

Fig. I-2. Sketch of a 7 × 12-mil rectangular InSb n-p junction diode, which has a 6 × 6-mil bonding pad.

One problem with this structure is that contact is made to the diodes over the active region, a process which leads to reduced yield. In order to investigate the array possibilities of this technique, we have fabricated a bonding pad structure as shown in Fig. I-2. The SiO_2 coating and gold contact to the n-type layer are deposited on the p-type substrate as in the previous structure, and the bombarded layer is defined using photoresist. Following the bombardment and removal of the photoresist, a chrome-gold metallization is deposited and photolithographically defined to provide a bonding pad out over the oxide and the inactive p-type substrate. The dimensions of this diode are 7 × 12 mils, with a 6 × 6-mil bonding pad.

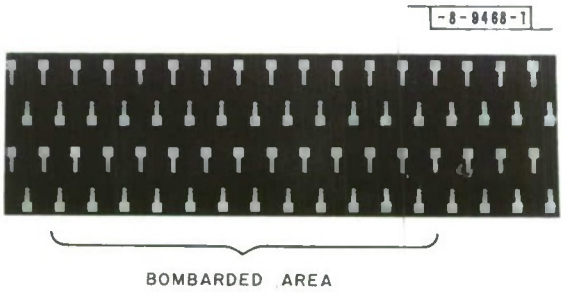

Fig. I-3. Photograph of an array of 7 × 12-mil InSb diodes fabricated using proton bombardment. There are two staggered linear array patterns on this sample, with 22 diodes from each array in the bombarded area. Each array pattern consists of two rows of diodes with a 10-mil offset between the rows. The center-to-center spacing between diodes in a row is 20 mils and the space between the active regions of the diodes in the two separate rows is 10 mils. In this figure, the gold bonding pads and contacts can be seen; however, the planar n-type regions cannot be distinguished from the p-type substrate.

A photograph of a sample prepared in this way is shown in Fig. I-3. There are two staggered linear array patterns on this sample, with 22 diodes from each array in the bombarded area. Each array consists of two rows of diodes with a 10-mil offset between the rows. The center-to-center spacing between diodes in a row is 20 mils, and the space between the active regions of the diodes in the two rows is 10 mils. In this figure, the gold bonding pads and contacts can be seen; however, the planar n-type regions cannot be distinguished from the p-type substrate. All 44 devices for this sample were good diodes, with zero-bias resistances between 200 and 460 kohms and capacitances from 32 to 42 pF at 77° K. Results are given in Table I-2. These devices have not yet been mounted for detectivity measurements; however, results on other samples of this array pattern, which have been mounted and evaluated, indicate that these diodes should have reduced background detectivities in the range consistent with their zero-bias resistances.

Diodes have also been fabricated using different surface coatings in an attempt to increase the device impedance. The results of one such experiment are outlined in Table I-3 where the parameters of two 15-mil-square diodes are compared. The first diode was fabricated using pyrolytic SiO_2 as the surface coating. The second diode was fabricated in the same way except that 1000 Å of evaporated ZnS was used instead of the SiO_2. As may be seen, the diode capacitances are about the same, but the zero-bias resistance of the second diode is much higher. The quantum efficiencies are comparable, and the detectivity of the ZnS-coated device reflects its larger resistance, with a peak value of 1.1×10^{12} cmHz$^{1/2}$/W at 4.8 μm. In the near future, we plan to fabricate and evaluate arrays of diodes on samples coated with ZnS.

TABLE I-2

ZERO-BIAS RESISTANCE VALUES (kahm) FOR THE 44 DIODES ON THE InSb SAMPLE SHOWN IN FIG. I-3

460	340	420	380	380	360	350	320	260	260	240
430	430	380	380	350	340	300	300	270	260	340
430	430	200	310	220	240	250	270	250	230	260
450	210	330	200	260	200	210	275	250	220	240

Diode Area = 5.25×10^{-4} cm^2

C(0) = 32 ta 42 pF

T = 77°K

TABLE I-3

COMPARISON OF InSb DIODES FABRICATED WITH DIFFERENT SURFACE COATINGS†

Surface Caating	SiO_2	ZnS
C (0) [pF]	78	75
R (0) [megahm]	0.25	4.0
η (λ = 4.8 μm) [percent]	30	26
D^*_λ (4.8 μm) [cm $Hz^{1/2}/W$]	3.0×10^{11}	1.1×10^{12}

T = 77°K

Diode Area = 1.4×10^{-3} cm^2

† The first diade was fabricated as in Fig. I-1 using pyralytic SiO_2 as the surface caating. The second diade was fabricated in the same way except that 1000 Å af evaporated ZnS was used instead af the SiO_2.

In conclusion, we have shown that the n-p junction diodes fabricated using proton bombardment are stable for periods exceeding a year, that they may be easily made in arrays and that the zero-bias resistance can be considerably increased using other surface coatings. We feel that these results show that this fabrication technique is a very attractive method for making InSb diode arrays.

A. G. Foyt
W. T. Lindley
J. P. Donnelly

B. TUNABLE $PbS_{1-x}Se_x$ DIODE LASERS NEAR $\lambda = 5\,\mu m$

1. Laser Characteristics

CW tunable diode lasers have been fabricated from vapor-grown single crystals of $PbS_{1-x}Se_x$ and the variation of their emission wavelength as a function of composition, current, temperature and magnetic field has been measured. These lasers represent a significant step in extending CW tunable laser operation from a previous short wavelength limit of $6.5\,\mu m$ for $Pb_{1-x}Sn_xTe$ to

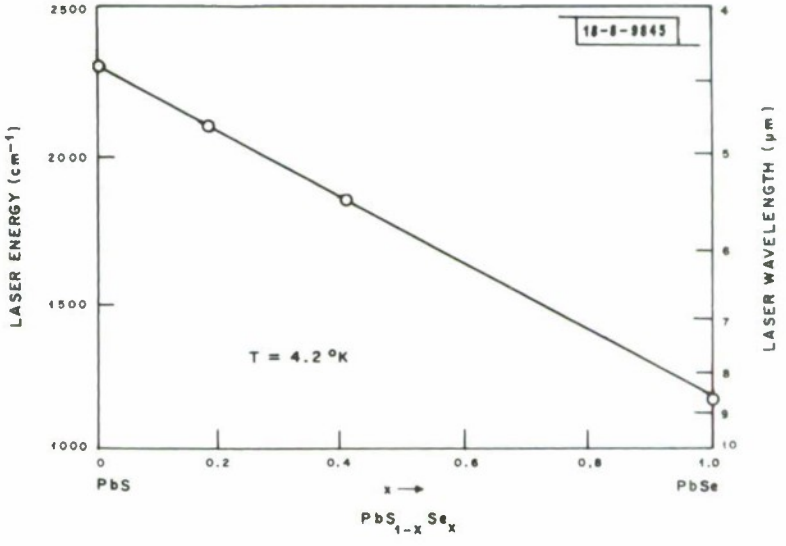

Fig. I-4. Emission wavelength for $PbS_{1-x}Se_x$ diodes with nominal composition x.

the region of $5\,\mu m$. The crystals were grown at 800°C from a metal-rich vapor phase in a sealed quartz ampoule as described in Ref. 2. The as-grown n-type crystals were isothermally annealed at 500°C for 7 days in the unopened growth ampoule. A p-type skin approximately $25\,\mu m$ deep was produced by a subsequent 1-hour diffusion at 550°C in the presence of a sulfur-selenium rich vapor. Fabry-Perot cavities were formed by cleaving along ⟨100⟩ planes with final dimensions of about $1 \times 0.3 \times 0.2$ mm. Figure I-4 illustrates the observed composition dependence of the laser wavelength for the $PbS_{1-x}Se_x$ system. The linear variation between PbS and PbSe is similar to that previously reported.[3] The temperature dependence of the center of the laser modes of a $PbS_{0.82}Se_{0.18}$ diode and a $PbS_{0.60}Se_{0.40}$ diode was measured between T = 1.8° and 50°K with the results shown in Fig. I-5a. Above T = 20°K the variation with temperature $\Delta\nu/\Delta T \approx 2.4\,cm^{-1}/°K$ is similar to that observed for other lead salt diode lasers. The tuning

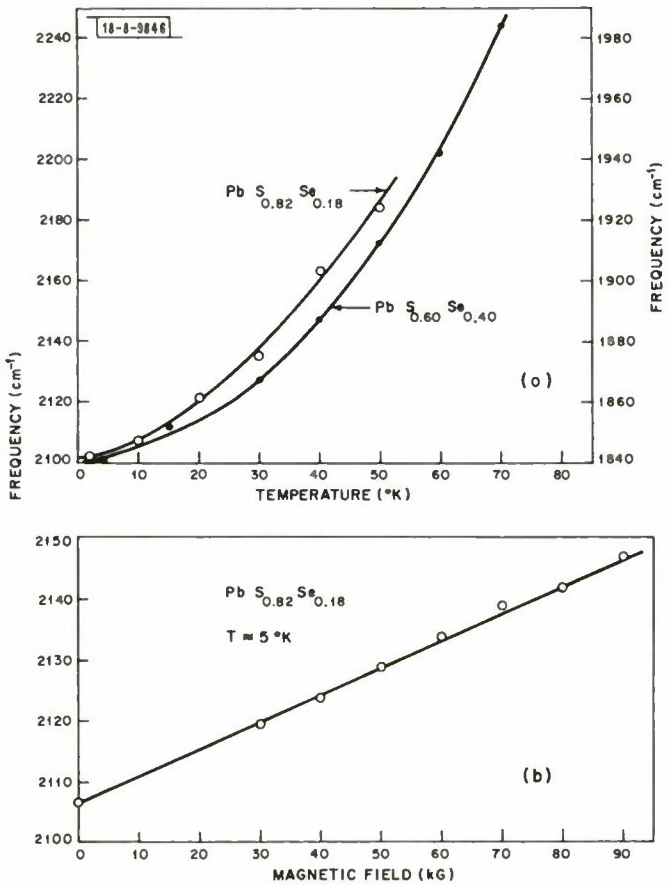

Fig. I-5(a,b). Temperature and magnetic field dependence of the emission wavelength of a $PbS_{1-x}Se_x$ diode loser.

of the center of the laser modes with magnetic field is shown in Fig. I-5b for the same $PbS_{0.82}Se_{0.18}$ diode. A rate of $\Delta\nu/\Delta H = 0.44\,cm^{-1}/kG$ is observed for the lowest energy interband transition with B || ⟨100⟩. The output spectra for this diode operating CW on the cold finger of a liquid helium dewar was nearly a single mode at a diode current of 450 mA with an output power of 8 μW measured from one end of the cavity. This dominant mode shifted at a rate of $d\nu/dI = 0.0083\,cm^{-1}/mA$ at I = 450 mA and could be tuned over a range of about $1\,cm^{-1}$. Note that this is the tuning rate of a single Fabry-Perot mode, whereas the temperature, magnetic field and composition tuning discussed above pertain to the gross motion of the Fabry-Perot mode pattern.

The expected linewidth of the mode at a total mode power of 16 μW is about $\Delta\nu = 0.00003\,cm^{-1}$ or 1 MHz.[4] This wide tunability and narrow linewidth were used for tunable infrared spectroscopy on CO gas discussed below.

2. Spectroscopy of Carbon Monoxide Gas

The output of a $PbS_{0.82}Se_{0.18}$ diode laser was current tuned through the P(9) absorption line of CO at $2107.4\,cm^{-1}$ (4.745 μm) with the results shown in Fig. I-6(a). This figure shows the

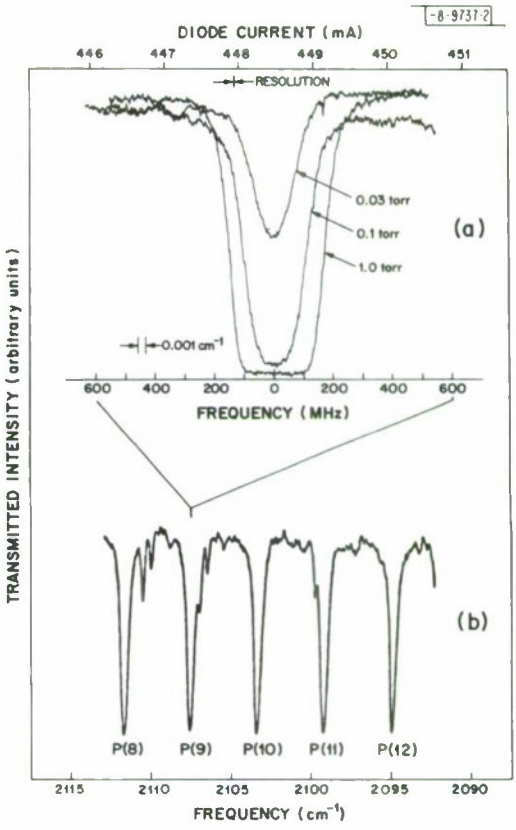

Fig. I-6(a,b). Transmission of CO gas: (a) spectra obtained using a current tunable $PbS_{0.82}Se_{0.18}$ laser; (b) spectra obtained using a conventional grating spectrometer.

transmission through a 10 cm cell filled with CO gas at a pressure of 1, 0.1 and 0.03 torr. The frequency axis is calibrated in terms of current and frequency using the tuning rate discussed above (250 MHz/mA). At a pressure of 1.0 torr the absorption cell is sufficiently long to produce total absorption over a range of frequency resulting in the flat portion of the transmission near line center. Reducing the pressure to 0.03 torr reveals the true Doppler linewidth from which a linewidth of 150 MHz and a line center absorption of 2.1 cm^{-1}/torr can be obtained. The calculated Doppler linewidth at T = 300° K is 148 MHz and the calculated absorption is 1.95 cm^{-1}/torr. Figure I-6(b) shows the absorption spectrum of CO taken with a grating spectrometer having a resolution of 0.3 cm^{-1}. The large improvement in resolution obtained through use of diode laser is apparent.

K. W. Nill A. R. Calawa
F. A. Blum T. C. Harman

C. PRELIMINARY RESULTS ON THE EPITAXIAL GROWTH OF $(In_xGa_{1-x})As$

A number of vapor-phase techniques have been used to grow (InGa)As alloys. Single crystal growth has been obtained by closed-tube halide transport of the binary compounds[5,6] and several open-tube flow systems have been used, including HCl transport of the elements with a metallic arsenic source,[6,7] HCl transport of the binary compounds[8] and HCl transport of the elements with an AsH_3 source.[9] Here we report preliminary results on the epitaxial growth of (InGa)As alloys of low indium composition using an In-Ga-$AsCl_3$-H_2 flow system.

TABLE I-4
ELECTRICAL PROPERTIES OF $(In_xGa_{1-x})As$

$n_{300°K}$ (cm^{-3})	$\mu_{300°K}$ ($cm^2/Vsec$)	$\mu_{77°K}$ ($cm^2/Vsec$)	t (μm)
9.2×10^{14}	7,100	60,000	83
2.3×10^{14}	6,500	72,000	65
1.4×10^{14}	5,500	52,000	73
3.1×10^{14}	6,400	49,000	41
3.0×10^{14}	5,600	45,000	47

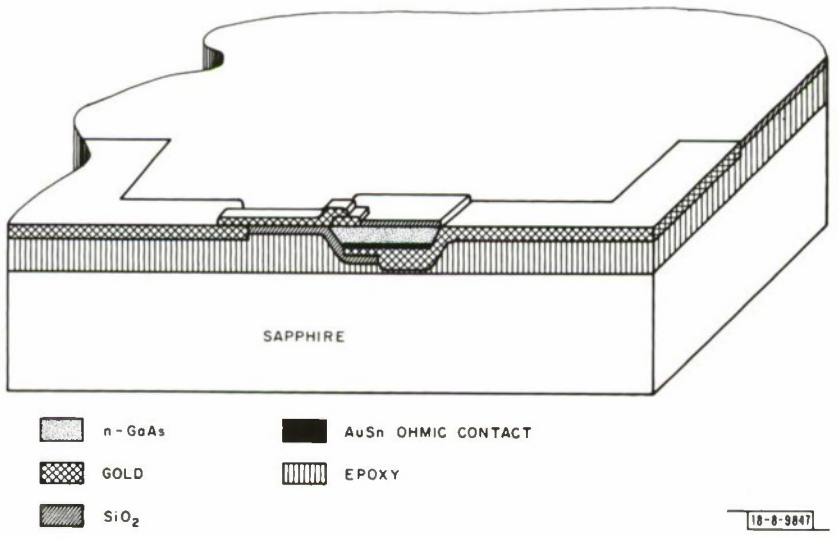

Fig. I-7. Cross-section of a double sided GaAs Schottky barrier microwave mixer diode.

These alloys were grown on GaAs substrates in a reactor identical to that previously used[10] to grow epitaxial GaAs. Growth conditions which are optimum for the growth of high-purity GaAs[10] were used with the In-Ga melt at 800°C and the GaAs substrates at 700°C. Under these conditions the layers were single-crystalline. Growth rates of about 0.2μ/min were obtained on {211}Ga surfaces.

Melt compositions from 0 to 60 atomic percent indium resulted in alloys with energy gaps from 1.39 to 1.33 eV, as determined from photoconductivity measurements. In this range of alloy compositions most of the strain due to lattice mismatch appeared to be elastic with no visual evidence of interfacial dislocations or planar defects. Unintentionally doped electron concentrations were in the $10^{14}\,cm^{-3}$ range. The electrical properties of several samples are listed in Table I-4. These layers are estimated[11] to have residual electrically-active impurity concentrations in the low $10^{15}\,cm^{-3}$ range.

C. M. Wolfe
L. Krohn, Jr.

D. DOUBLE SIDED GaAs SCHOTTKY BARRIER MICROWAVE MIXER DIODES

We have developed a technique for fabricating GaAs Schottky barrier diodes suitable for use as 50 GHz mixers. The goal of this program is to fabricate these diodes, complete with their external connections, while at the same time minimizing parasitic parallel capacitances, series resistance and series inductance. Preliminary results indicate that this device can be made using the double-sided fabrication technique which is also being used to fabricate GaAs Schottky barrier field effect transistors.[12]

A cross section of the device is shown in Fig. I-7. Fabrication is accomplished in two distinct series of steps dealing with the two sides of the GaAs layer. The first side fabrication starts with a polished piece of bulk n-type GaAs of the appropriate carrier concentration (1 to $5 \times 10^{17}\,cm^{-3}$). This piece has photolithographically-defined ohmic contacts applied in appropriate regions using 300 Å of electroplated 25 percent tin and 75 percent gold alloy. The contacts are alloyed at 540°C in a hydrogen and hydrogen chloride atmosphere. Additional gold is plated onto these ohmic contacts which will eventually become the back contacts for the diodes. The contacts are now used as an etch mask to etch 1 × 3 mil, 2-μm-high mesas in the GaAs. These mesas will be the only GaAs remaining in the final device. Additional gold is plated onto the GaAs to form the connecting metallization in the final device.

The piece of GaAs in now epoxied onto a sapphire substrate. The wafer and substrate are joined in a vacuum and forced together with pressure to provide a thin glue line with no trapped air bubbles. The fabrication of the second side of the device now proceeds with the lapping, polishing and etching away of most of the GaAs leaving only the previously defined mesas, which are now pockets of GaAs about 2μm thick. The surface of the sample is now coated with a low temperature pyrolytic silicon oxy-nitride and openings are defined for the electroplated 3 × 6-μm-wide gold Schottky barrier diodes. The final step is to open appropriate regions through the silicon oxy-nitride to the previously formed gold contact metallization and also to evaporate additional gold over the sample and to define in this gold a 3-μm-wide bridge connecting the Schottky barrier diode to the contact metallization.

Measurements which have been made at low frequencies on the initial diodes fabricated by this process indicate that diodes with zero-bias capacitances of 0.020 to 0.030 pF can be fabricated

with parasitic capacitances, due to the contact bridge and metallization, of less than 0.010 pF. The DC series resistance of these diodes is 30 to 50 ohms.

W. T. Lindley
C. E. Hurwitz

E. GaAs ACOUSTIC SURFACE WAVE DELAY LINES

Several 270-MHz acoustic surface wave delay lines have been made on semi-insulating GaAs. Two gold interdigital electrode transducers with thirty 0.1-mil finger pairs were fabricated onto a (100) surface, aligned along the [011] axis and separated by 200 mils. Although a maximum effective coupling occurs in this configuration, the surface wave excited is the limiting case of a leaky waveform; hence, one might expect extensive propagation losses.[13]

A two-way insertion loss of 21 dB was measured for all three 1.8-μsec delay lines tested, using simple inductor tuning. Electrical mismatch between the 50-ohm RF generator and the low impedance (~5 ohms) of the transducers and their bidirectional nature (6 dB loss) could account for most, if not all, of this loss. Using double-stub tuners we were able to reduce the insertion loss to 15 dB. The 3-dB bandwidth was found to be 5 MHz and the triple transit signal was down 18 dB, which is consistent with the measured insertion loss.

A longer delay line (400 mils, 3.6 μsec) with an open transducer in the path of propagation was found to have only 1 dB additional loss, indicating that propagation losses for this cut of GaAs are less than 0.5 dB/μsec at 270 MHz. Higher frequency transducers are being made to get a more exact value for these losses.

D. L. Spears

F. X-RAY LITHOGRAPHY

A program has been undertaken to develop a process utilizing x-radiation to replicate extremely high resolution microelectronic patterns. These submicron structures will be written with a scanning electron microscope into specially designed x-ray pattern masks. Such patterns can then be reproduced an unlimited number of times since the large spacing between the mask and wafer, allowable with x-rays, greatly reduces the chance of damage to the pattern mask.

The problems and limitations experienced in the field of contact microradiography have served as a guide.[14] To obtain adequate transmission contrast in a thin film pattern mask, one must use soft x-rays (~10 Å), which are very inefficiently produced by conventional x-ray tubes. The most promising means of imprinting the submicron patterns is by radiation degradation of organic polymers, recording media some seven orders of magnitude less sensitive than ordinary x-ray film. Consequently, sufficient x-ray source intensity is of primary concern.

Studies of the sensitivity of polymethyl methacrylate (PMM) to 1.5- and 2.3-Å radiation have been made and a dose on the order of 50 Mrad (~500 J/cm^3) was found necessary to render the material readily soluble in 40 percent methyl isobutyl ketone and 60 percent isopropyl alcohol. The solubility of PMM varied as the 3rd power of the exposure time in this dose range, indicating that a contrast of 10 to 1, or less, in the pattern mask should produce sharp images. Exposure times of several hours were required. Presently, more intense soft x-ray sources and methods for increasing the polymer sensitivity by doping it with an element which absorbs x-rays more efficiently, are being researched.

D. L. Spears
H. I. Smith
E. Stern

REFERENCES

1. Solid State Research Report, Lincoln Laboratory, M.I.T. (1969:4), p. 3.
2. J. F. Butler and T. C. Harman, Appl. Phys. Letters 12, 347 (1968), DDC AD-673601.
3. S. P. Chashchin, I. S. Aver'yanov and N. S. Bargshev, Fiz. i Tek. Polup. 4, 1794 (1970) [Soviet Phys. – Semiconductors 4, 1538 (1971)]; L. N. Kurbatov, A. D. Britov, I. S. Aver'yanov, V. E. Mashchenko, N. N. Mochalkin and A. I. Dirochka, Fiz. i Tek. Polup. 2, 1200 (1968) [Soviet Phys. – Semiconductors 2, 1008 (1969)].
4. E. D. Hinkley and Charles Freed, Phys. Rev. Letters 23, 277 (1969), DDC AD-694147.
5. R. Sirrine, J. Electrochem. Soc. 111, 750 (1964).
6. H. T. Minden, J. Electrochem. Soc. 112, 300 (1965).
7. R. W. Conrad, P. L. Hoyt and D. D. Martin, J. Electrochem. Soc. 114, 164 (1967).
8. E. W. Mehal and G. R. Cronin, Electrochem. Tech. 4, 540 (1966).
9. R. E. Enstrom, D. Richman, J. Appert, D. G. Fisher, A. H. Sommer and B. F. Williams, Proc. 3rd Int. Symp. GaAs (Inst. Phys. Physical Soc., London, 1971), pp. 30-40.
10. C. M. Wolfe and G. E. Stillman, Proc. 3rd Int. Symp. GaAs (Inst. Phys. Physical Soc., London, 1971), pp. 3-17.
11. C. M. Wolfe, G. E. Stillman and J. O. Dimmock, J. Appl. Phys. 41, 504 (1970), DDC AD-707572.
12. Solid State Research Report, Lincoln Laboratory, M.I.T. (1970:2), p. 7.
13. J. J. Campbell and W. R. Jones, J. Appl. Phys. 41, 2796 (1970).
14. G. L. Clark, The Encyclopedia of Microscopy (Reinhold, New York, 1961).

II. MATERIALS RESEARCH

A. INSULATING MATERIALS FOR HIGH TEMPERATURE FURNACES

The principal mechanism of heat loss from furnaces operating above about 600° K is the radiation of energy in the infrared region of the spectrum. If the heat source is surrounded by multiple concentric metal heat shields [Fig. II-1a)], this loss can be reduced by orders of magnitude. Each shield acts by absorbing radiation from the hotter side and reemitting it in both directions, causing a net reduction in the heat loss from the source. Although the radiation path is more complicated, fibrous and packed insulations [Fig. II-1(b)] operate in a similar manner.

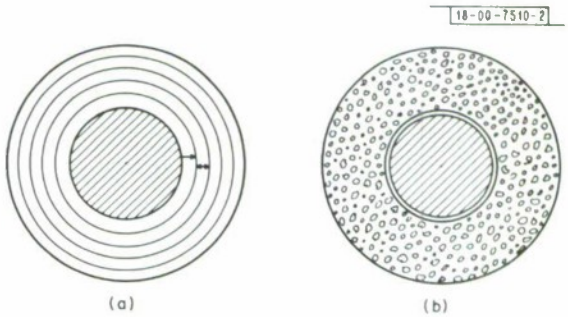

Fig. II-1. (a) Multiple radiation shields and (b) fibraus or packed insulatian far high temperature furnaces.

For crystal growth and thermal analysis at high temperatures we use a furnace consisting of a tungsten heating element insulated from a water-cooled shell by five heat shields.[1] The shields are made from tantalum (mp = 3250° K) or molybdenum (mp = 2890° K), since these metals are available in thin sheets which are easily cut and formed into the required shapes. However, the fabrication of the multiple shields is tedious and expensive because it is necessary to space the individual shields in order to reduce the contact between them as much as possible. If fabrication could be made more convenient, it would be feasible to reduce heat losses still further by greatly increasing the number of shields. This would make it possible to reach higher temperatures with less power and achieve a closer approach to black-body conditions in the furnace. Thus, a commercial furnace which uses up to 50 shields, made of tungsten sprayed with a layer of ZrO_2 acting as spacer material, is capable of reaching 2200° C in a 6-inch-diameter × 8-inch-high hot zone with 1.6 kW of power, although it cannot operate at much higher temperatures because of the instability of the ZrO_2.

Fig. II-2. Embossed tantalum heat shields 10 layers thick.

We have investigated the possibility of using multiple heat shields made from tantalum sheet 0.005 inch thick which has been embossed by a commercial rolling process to an overall thickness of 0.030 inch. Ten turns of this material were tightly wound in a spiral to form the cylinder shown in Fig. II-2, which was spot welded to prevent unwinding. The only spacing between the turns was that due to the roughness resulting from embossing. Two stacks, each containing 10 discs of the same material, were spot welded to form

TABLE II-1

POWER REQUIREMENTS FOR DIFFERENT INSULATIONS IN HIGH TEMPERATURE FURNACE

Insulation		Power to Reach 2500°K (kW)	n in $P \approx T^n$
1 Ta shield	Vacuum	7.6	4.64
	Argon	8.1	4.60
5 Ta shields	Vacuum	3.75	4.26
	Argon	4.1	4.22
10 embossed Ta shields	Vacuum	2.5	4.24
	Argon	3.05	4.87
5-mm thick fibraus ZrO_2	Vacuum	4.8	5.21
	Argon	(4.9)*	4.13

*Extrapalated

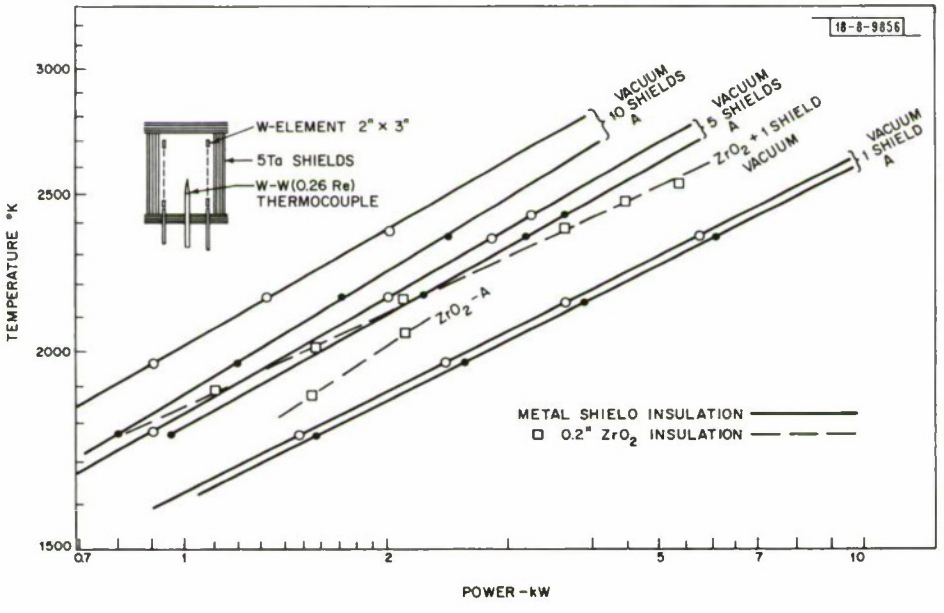

Fig. II-3. Pawer vs temperature far metal heat shield and fibrous zirconia insulatian.

the upper and lower insulators also shown in Fig. II-2. To test the effectiveness of this easily constructed unit, it was substituted for the usual heat shields in the crystal growth furnace, and the power required to reach various temperatures was measured. The data obtained for operation in vacuum and in argon are plotted in Fig. II-3, together with the results of similar tests with either 1 or 5 conventional tantalum heat shields. For each configuration the power required increases with temperature according to the expression $P = T^n$. The measured power values and the numerical values of the exponent n are listed in Table II-1. Replacing the 5 individual shields with the 10-shield unit decreased the power required to reach a given temperature by about 35 percent in vacuum and in argon.

Stabilized ZrO_2 in felt form has recently become available. As an alternative to multiple heat shields, an insulating unit was made by winding a single layer of this felt (0.5 cm thick) around a single tantalum shield for support and placing similar combinations of a layer of felt and a single tantalum shield at the top and bottom. The results of tests on this unit, represented by the dashed curves in Fig. II-3, show that a single layer of felt is equivalent to several metal heat shields. The zirconia performed well in vacuum up to 2550° K; but in argon, decomposition appeared to occur at lower temperatures and the tantalum supports were embrittled by contact with the zirconia.

T. B. Reed
R. E. Fahey

B. HIGH-PRESSURE SYNTHESIS OF $BiRhO_3$, A NEW PEROVSKITE

The reaction of Bi_2O_3 with either Rh metal or Rh_2O_3 (Bi/Rh = 1) at 600° to 1000°C in air or oxygen forms a compound with the face-centered-cubic pyrochlore structure (a = 10.24 Å) (see Ref. 2). Its composition is $Bi_{2.0}Rh_{2.0}O_{6.8}$, based on x-ray fluorescence data for the Bi/Rh ratio and thermogravimetric data for the oxygen content.

The reaction of a stoichiometric mixture of Bi_2O_3 and Rh_2O_3 in a sealed, evacuated quartz tube at 750° to 1000° C yields a product that has not been identified. When the same mixture is placed in a platinum capsule and subjected to over 65 kbar pressure at 1000° to 1300° C for one-half hour, the orthorhombic perovskite $BiRhO_3$ is formed. The peak positions of the x-ray diffraction lines for this compound were taken from a 1/4 deg/min diffractometer tracing obtained by using monochromated (graphite crystal) CuK_α radiation. The dimensions of the orthorhombic cell found by refinement of these data are a = 5.354 ± 0.005 Å, b = 5.813 ± 0.005 Å and c = 7.776 ± 0.005 Å. The observed peak intensities are in good agreement with those calculated for this unit cell by using the position parameters determined by Geller[3] for the perovskite $GdFeO_3$.

J. A. Kafalas
J. W. Pierce
J. M. Longo

C. CRYSTALLOGRAPHIC TRANSITIONS IN $V_{1-x}Cr_xO_2$

It has been known for over a decade that VO_2 exhibits a first-order semiconductor-to-metal transition at $T_t \approx 340°$ K. Electrical-resistivity discontinuities as large as five orders of magnitude have been observed. High-temperature VO_2 has the tetragonal ($P4_2/mnm$) rutile structure illustrated in Fig. II-4.

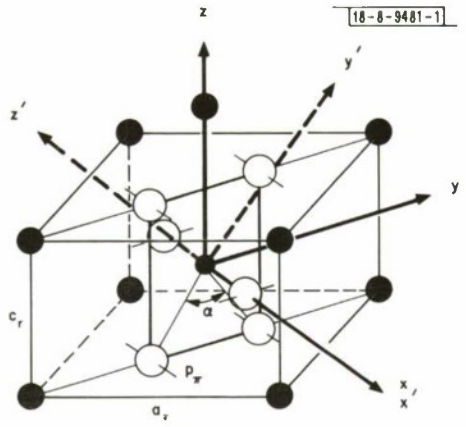

Fig. II-4. Tetrogonal, rutile structure. Open circles represent O^{2-} ions with orientation of p_π orbitals, closed circles V^{4+} ions.

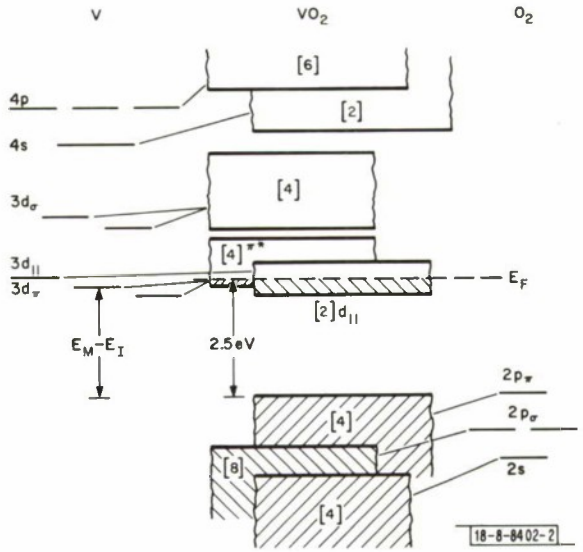

Fig. II-5. One-electron bond structure for tetrogonol VO_2.

Construction of an energy-level diagram for tetragonal VO_2 is shown schematically in Fig. II-5. The O^{2-}:2p orbitals are stabilized relative to the V^{4+}:3d orbitals by the energy $(E_M - E_I)$, where E_M is the Madelung energy for the effective charges on the ions and E_I is the ionization energy of the cation minus the electron affinity of the anion. The one-electron ionic energy levels, including crystal-field splittings, are indicated on the left and right sides of the figure. From experiments on the perovskites,[4] it is known that the $d_\pi - O^{2-}$:$p_\pi - d_\pi$ interactions are strong enough to break down the conditions for localized d_π electrons, so that the d_σ and d_π orbitals must be represented as itinerant-electron, σ^* and π^* band orbitals. Furthermore, the cation-cation separation between nearest-neighbor cations along the c_r axis is $R < R_c \approx 2.94$ Å, where R_c is a semiempirical critical separation for localized vs itinerant 3d electrons in oxides,[5] and the $d_{||}$ electrons must form a cation-sublattice band of itinerant-electron states. Since the widths of the $d_{||}$ and π^* bands should be larger than any crystal-field splitting due to the deformation of the octahedral-site geometry from cubic to orthorhombic symmetry, the $d_{||}$ and π^* bands must overlap. From the nearly isotropic conductivity and an anomalous variation of the c_r/a_r ratio with temperature, it may be inferred that these two overlapping bands are each partially occupied, as indicated in Fig. II-5. Placement of the Fermi energy relative to the edge of the π band was obtained from comparisons of the optical reflectance and absorption spectra of VO_2 and TiO_2.

Given the band structure of Fig. II-5, a transition from a metallic to a semiconducting state requires two distinguishable changes: (1) a raising of the π^* bands above the Fermi energy E_F, thus leaving the $d_{||}$ band half-filled, and (2) a splitting of the $d_{||}$ band. Such a change in the d bands is illustrated in Fig. II-6.

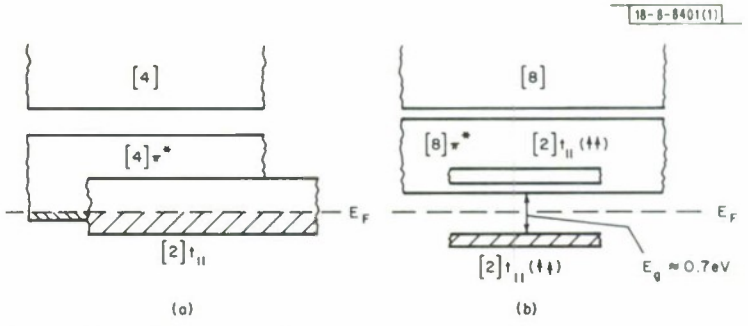

Fig. II-6. Schematic modification of d-band structure on passing from metallic to semiconducting phase: (a) tetragonal VO_2; (b) monoclinic V_2O_4.

Raising of the π^* bands above E_F requires either a destabilization of the π^* bands or a stabilization of at least the bottom half of the $d_{||}$ band or both. Destabilization of the π^* bands would result from a crystallographic distortion that increases the splitting between the π and π^* bands. Stabilization of the $d_{||}$ bands would be induced by a decrease in the axial ratio c_r/a_r. The bottom half of the $d_{||}$ band would be stabilized by a doubling of the c_r axis, either through a crystallographic distortion or magnetic ordering, since such a doubling of the c_r axis would split the $d_{||}$ band in two.

Low-temperature VO_2 has the monoclinic ($P2_1/c$) structure of Fig. II-7. A striking feature of this monoclinic phase is the presence of cation-cation pairs along the $a_m = 2c_r$ axis, alternate V-V separations being 2.65 Å < R_c and 3.12 Å > R_c in place of the regular 2.87 Å spacing in the tetragonal phase just above the transition temperature T_t. This feature immediately suggests metal-metal bonding. The narrow-band requirements for a transition from narrow bands to cation clusters have been shown to be satisfied by the $d_{||}$ bands of VO_2 (see Ref. 5). A second significant feature of the low-temperature structure is a tilting of the c_r-axis V-V pairs to give one shortest vanadium-oxygen separation R_{VO} = 1.76 Å perpendicular to the c_r axis. The two bridging oxygens between paired vanadium ions have $R_{VO} \approx 1.86, 1.87$ Å. The other three cation-anion distances are 2.01, 2.03 and 2.05 Å. The displacement of a cation from the center of its interstice toward one or more anions is characteristic of a ferroelectric-type distortion. This feature of the monoclinic phase suggests that an antiferroelectric distortion coincides with the formation of V-V homopolar bonds below T_t. Therefore the driving mechanism responsible for the transition at T_t may be an antiferroelectric transition rather than the formation of homopolar-bonded V-V pairs, or it might be a complex combination of the two mechanisms.

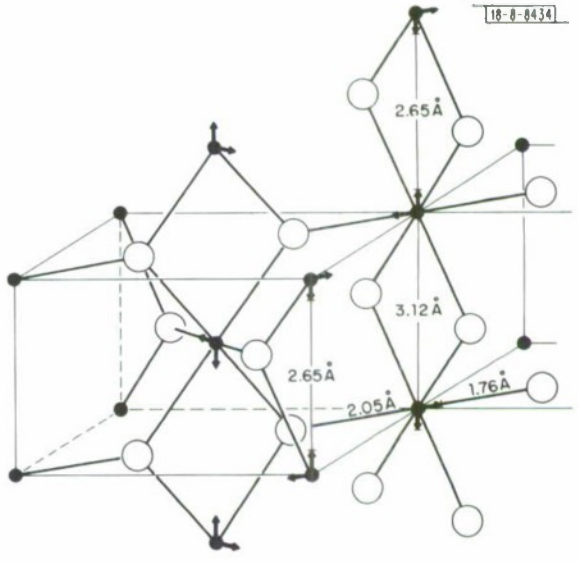

Fig. II-7. Monoclinic structure of low-temperature VO_2 and its relationship to the rutile structure.

TABLE II-2

INITIAL RATE OF CHANGE OF UPPER TRANSITION TEMPERATURE WITH COMPOSITION (dT_t/dx) FOR THE SUBSTITUTIONAL COMPOUNDS $V_{1-x}M_xO_{2+\epsilon}$, WHERE ϵ IS UNSPECIFIED AND PRESUMED ZERO

[Critical compositians x_1 and x_2 indicate phase changes at room temperature. Raom-temperature structures within the regians $x_1 < x < x_2$ and $x > x_2$ are also indicated, where mana. refers ta the manaclinic ($P2_1/c$) phase of Fig. II-7 and ortho. ta the ortharhombic (probable space graup F222) phase af Fig. II-9].

M	dT_t/dx [°K/at % M]	x_1	x_2	$x_1 < x < x_2$	$x > x_2$
Cr^{3+}	~+3	0.01	0.20	ortho.	(2φ)*
Fe^{3+}	+3	0.01	0.125	ortha.	two-phase
Ga^{3+}	+6.5	0.005	0.02	ortha.	twa-phase
Al^{3+}	+9.0	0.005	0.045	artha.	two-phase
Ti^{4+}	−0.5 to −0.7	0.2	0.2 ta 0.25	ortha.	rutile and (2φ)*
Re^{4+}	~−4	0.07		rutile	
Ir^{4+}	~−4	0.04	0.5	rutile	twa-phase
Os^{4+}	−7	0.03	0.1	rutile	two-phase
Ru^{4+}	−10	0.025	0.75	rutile	twa-phase
Ge^{4+}	+5				
Nb^{5+}	−7.8	0.05	0.9	rutile	NbO_2
Ta^{5+}	−5 ta −10	0.02	0.5	rutile	two-phase
Mo^{6+}	−5 to −10	0.03	0.55	rutile x = 1.0	(2φ)* mana.
W^{6+}	−28	0.013	0.68	rutile	ortha.

ordered trirutile phase about x = 0.33; $0.78 < x < 0.8$ (2φ')* phase; $0.85 < x < 1$ mana.

* The 2φ phase is a distorted rutile structure with arthorhombic symmetry, and the 2φ' phase is similar but with monaclinic symmetry.

Various workers have attempted to shift the transition temperature T_t with chemical doping. The rate of change of T_t with dopant concentration x is summarized in Table II-2. A striking feature of this Table is the appearance of an orthorhombic phase with substitution of M^{3+} ions, creating $V^{4+}_{1-2x}V^{5+}_{x}M^{3+}_{x}O_2$. Since neither the foreign M^{3+} ions nor the V^{5+} ions can participate in the formation of homopolar V-V bonds along the c-axis, such substitutions must suppress this aspect of the cooperative deformation found in low-temperature VO_2. The small V^{5+} ion, on the other hand, is notorious for its displacement from the center of symmetry of an oxygen octahedral site, and the antiferroelectric-type aspect of the cooperative monoclinic distortion may even increase with x, this increase being larger the smaller the M^{3+} ion and the stronger its tetrahedral-site preference energy. This idea is supported by the fact that of the M^{4+}-ion substitutions, only Ti^{4+}, which participates in ferroelectric distortions in $BaTiO_3$, and Ge^{4+} which has a strong tetrahedral-site preference energy, introduce the orthorhombic phase or increase T_t. M^{5+} and M^{6+} ions introduce charge carriers which suppress both components of the distortion, so that they cause T_t to decrease rapidly.

Actually, substitution of M^{3+} ions introduces two phase transitions, a monoclinic-to-orthorhombic transition at T_t' and an orthorhombic-to-tetragonal transition at T_t, as can be seen from Fig. II-8. According to our reasoning above, the orthorhombic phase should be primarily – if not entirely – due to an antiferroelectric-type displacement of the cations. In order to check this hypothesis, a structure refinement of the orthorhombic phase was undertaken. Powder-pattern intensitites of a carefully prepared and analyzed sample of $V_{0.95}Cr_{0.05}O_2$ were measured, and refinement of variable atomic-position parameters and cell temperature factor was made using a simplex program that minimized the usual discrepancy factor $R = 100\ \Sigma_i |I_i^{calc} - I_i^{obs}| / \Sigma_i I_i^{obs}$. The real and imaginary parts of the anomalous dispersion were taken into account.

The resulting structure is shown in Figs. II-9 and 10(a, b). The probable space group is F222, and the lattice parameters found were $a_o = 13.015$ Å, $b_o = 12.597$ Å and $c_o = 5.795$ Å. Comparison with the high-temperature rutile cell shows $a_o \approx 2\sqrt{2}\, a_r$ and $c_o \approx 2c_r$. The 32 vanadium and 64 oxygen atoms in the cell were assigned positions consistent with the rutile lattice and space group F222. This gave the assignments shown in Table II-3.

The complex orthorhombic structure consists of four distinguishable chains of edge-shared octahedra along the $c_o \approx 2c_r$ axis. Along the first chain, V_1 and V_2 positions are distinguishable by their different R_{VO} separations. The V_3 and $V_{3'}$ positions in the second chain are distinguished by antiferroelectric displacements along a_o; and the V_4 and $V_{4'}$ positions of the third chain by antiferroelectric displacements along b_o. Only in the fourth chain does V-V homopolar bonding occur, and without any attendant antiferroelectric displacement along b_o. This finding shows that the driving force for the transition at T_t is complex, involving both aspects of the distortion, and that the orthorhombic phase can indeed be interpreted as due to a larger antiferroelectric-type component than the homopolar-bond component to the crystallographic deformation.

J. B. Goodenough
J. W. Pierce

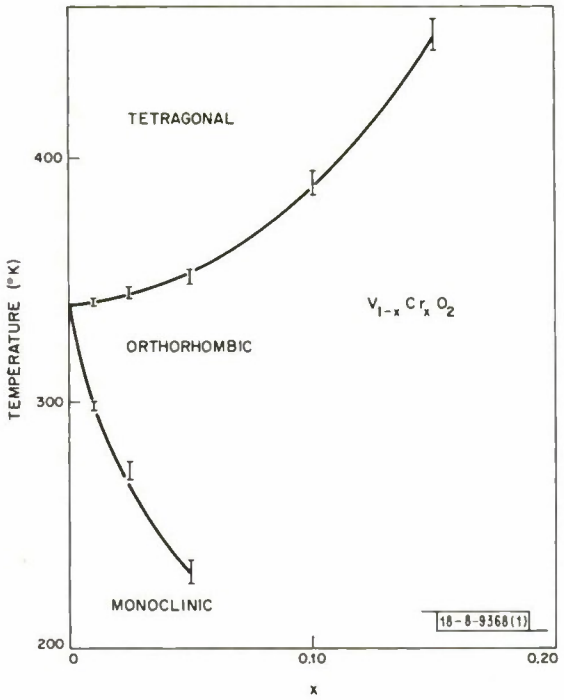

Fig. II-8. Phase diagram of $V_{1-x}Cr_xO_2$ system, after G. Villeneuve, A. Bordet, A. Casalot and P. Hagenuller, Mater. Res. Bull. 6, 119 (1971).

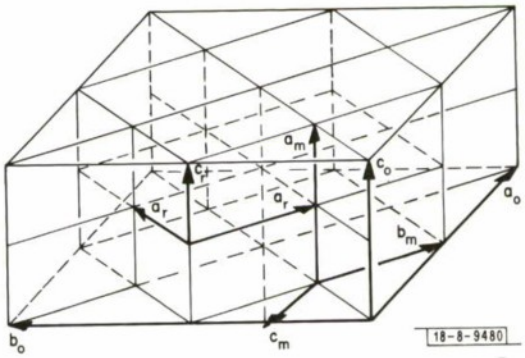

Fig. II-9. Relationship of tetrogonal ond monoclinic phoses to the orthorhombic phose of $V_{1-x}Cr_xO_2$.

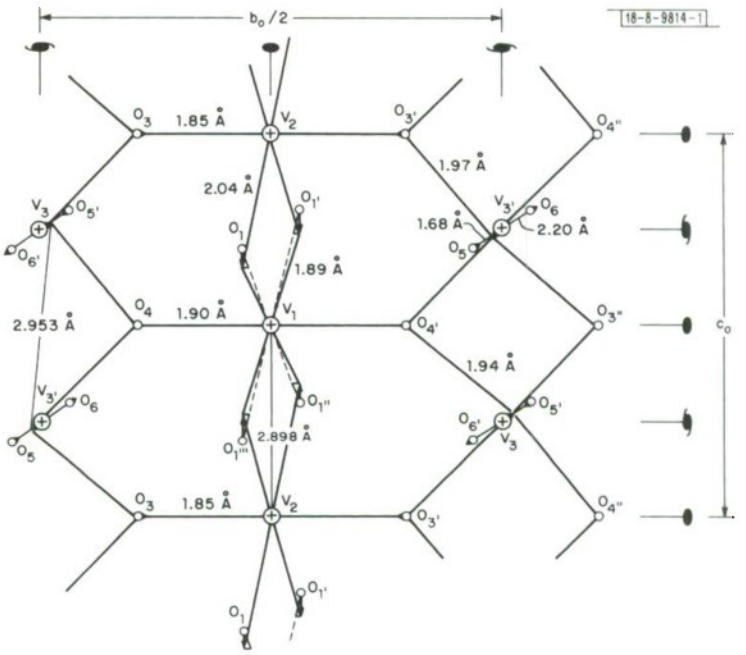

(a)

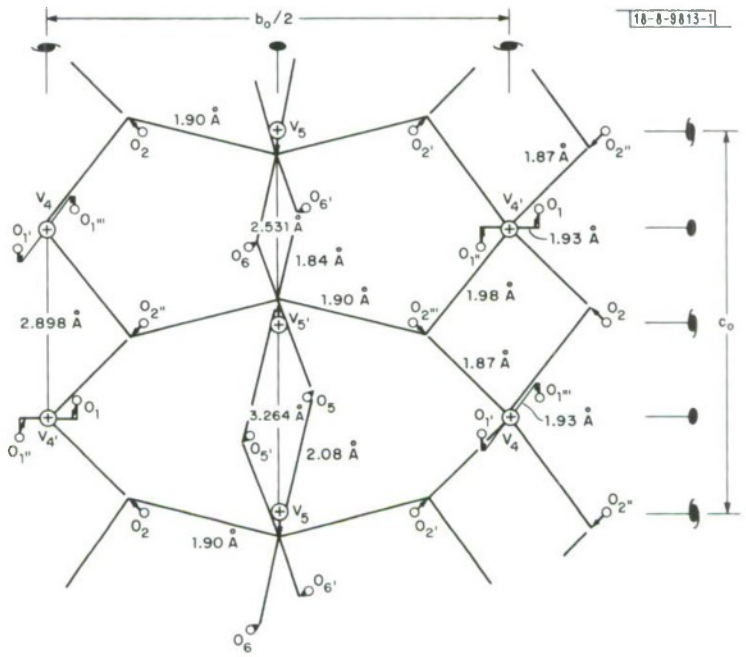

(b)

Fig. II-10. Atomic displacements from tetragonal structure and interatomic distances found in orthorhombic $V_{0.95}Cr_{0.05}O_2$, where (a) and (b) represent adjacent b-c planes.

TABLE II-3

CRYSTAL STRUCTURE OF ORTHORHOMBIC $V_{0.95}Cr_{0.05}O_2$

[Space group: F222; Unit cell dimensions: $o_o = 13.015$ Å, $b_o = 12.597$ Å, $c_o = 5.795$ Å; Cell content: $16(V_{0.95}Cr_{0.05})_2O_4$]

V_1 in 4a	(0, 0, 0)	
V_2 in 4b	$(0, 0, \frac{1}{2})$	
V_3 in 8j	$(x, \frac{1}{4}, \frac{1}{4}; \frac{1}{2}-x, \frac{1}{4}, \frac{1}{4})$	x = 0.0218
V_4 in 8i	$(\frac{1}{4}, y, \frac{1}{4}; \frac{1}{4}, \frac{1}{2}-y, \frac{1}{4})$	y = 0.0024
V_5 in 8h	$(\frac{1}{4}, \frac{1}{4}, z; \frac{1}{4}, \frac{1}{4}, \frac{1}{2}-z)$	z = 0.0316
O_1 in 16k	$(x, y, z; x, \bar{y}, \bar{z}; \bar{x}, y, \bar{z}; \bar{x}, \bar{y}, z)$	x = 0.1020, y = 0.0074, z = 0.2325
O_2 in 16k		x = 0.2515, y = 0.1004, z = 0.0089
O_3 in 8f	$(0, y, 0; 0, \bar{y}, 0)$	y = 0.1506
O_4 in 8f		y = 0.3533
O_5 in 8j	$(x, \frac{1}{4}, \frac{1}{4}; \frac{1}{2}-x, \frac{1}{4}, \frac{1}{4})$	x = 0.1506
O_6 in 8j		x = −0.1473
Crystol temperature factor = 1.3		

D. CRYSTAL GROWTH OF $Fe_{1-x}Cu_xCr_2S_4$ Alloys

The compounds $FeCr_2S_4$ and $CuCr_2S_4$ crystallize in the spinel structure with the normal cation distribution. $FeCr_2S_4$ is a semiconductor which exhibits ferrimagnetic ordering below ~190° K, while $CuCr_2S_4$ has metallic electrical properties and exhibits ferromagnetic ordering below ~400° K. Haacke and Beegle[6,7] showed that these compounds form a complete series of solid solutions, $Fe_{1-x}Cu_xCr_2S_4$. In the present study, our objectives are to grow single crystals across the entire composition range, to characterize them by chemical analysis and lattice parameter measurements, and to determine their electrical, magnetic and optical properties.

Powders of the alloys were prepared by mixing and pelleting 20 gram batches of the appropriate quantities of the elements and firing the pellets at 725° C in evacuated and sealed heavy-walled fused silica ampules for two to four 48-hour cycles. The product of the final firing was an easily crushed gray powder mixed with free S, which was generally removed from the crushed material by a series of washes with CS_2. The powders were characterized by x-ray diffraction and by chemical analysis for the four elements. They all contained substantially more S than the stoichiometric formula specifies. Data for representative samples are given in Table II-4.

To grow single crystals from these powders we have used the vertical transport method of Pinch,[8] which employs anhydrous $CrCl_3$ as the transport agent. The $CrCl_3$ is so hygroscopic that it must be handled in a dry box. Crystal growth takes place in a 23 to 29 mm o.d. fused silica tube 11 cm long. About 2 grams of alloy feed powder and 0.02 to 0.04 g of $CrCl_2$ are loaded into the tube which is evacuated and sealed. The growth tube is placed in the horizontal resistance-heated furnace shown schematically in Fig. II-11. At the start of a run, the top of the tube is raised to 860° to 880°C for at least 24 hours to drive off any of the powdered feed material which might have adhered to the walls in handling. The bottom is then raised to ~860° C, and the top is slowly lowered to below 860° C to initiate growth on the upper surface of the tube. In a typical run, the bottom is kept at 860 ± 2° C, while the top is lowered to 820 ± 2° C for a final ΔT of 40° C.

Although the growth variables were not studied separately in enough detail to get a quantitative measure of the effect of each, certain qualitative trends have been observed. As expected, more $CrCl_3$, longer periods at final ΔT, and higher feed temperatures gave greater amounts of transport. The largest single crystals and the largest number of usable crystals were obtained from runs with up to 25 percent transport. Four of the six best runs were made with feed material which had not been leached with CS_2.

The transported $Fe_{1-x}Cu_xCr_2S_4$ forms deposits of three types. The most frequent of these is a band or area of fine crystals which increase in size toward the bottom of the tube, so that crystals with edges >1 mm long may grow nearest the feed. The second form, found in the more successful runs, consists of individual crystals, up to 5 mm on an edge, which were nucleated and grown in isolation. The yield of such crystals from a typical good run is shown in Fig. II-12. The large flat faces are {111} planes, as observed by Pinch.[8] The third type of deposit consists of clusters of sizable crystals growing from a single spot (Fig. II-13).

TABLE II-4

PROPERTIES OF AS-PREPARED $Fe_{1-x}Cu_xCr_2S_4$ POWDERS

Composition				Lottice Constont (Å)	Notes
Relotive Number of Atoms					
Fe	Cu	Cr	S		
1.00	0	1.98	4.18	9.989	
0.70	0.30	2.04	4.19	9.936	
0.59	0.41	1.97	4.14	9.920	
0.55	0.45	1.99	4.14	9.909	
0.49	0.51	2.04	4.41	9.902	Not CS_2 leoched
0.49	0.51	2.00	4.16	9.903	
0.46	0.54	2.19	4.44	9.901	Not CS_2 leoched
0.39	0.61	2.01	4.18	9.885	
0.38	0.62	2.03	4.10	9.883	
0.36	0.64	2.11	4.43	9.880	Not CS_2 leoched
0.32	0.68	2.04	4.32	9.870	
0	1.00	2.06	4.24	9.819	

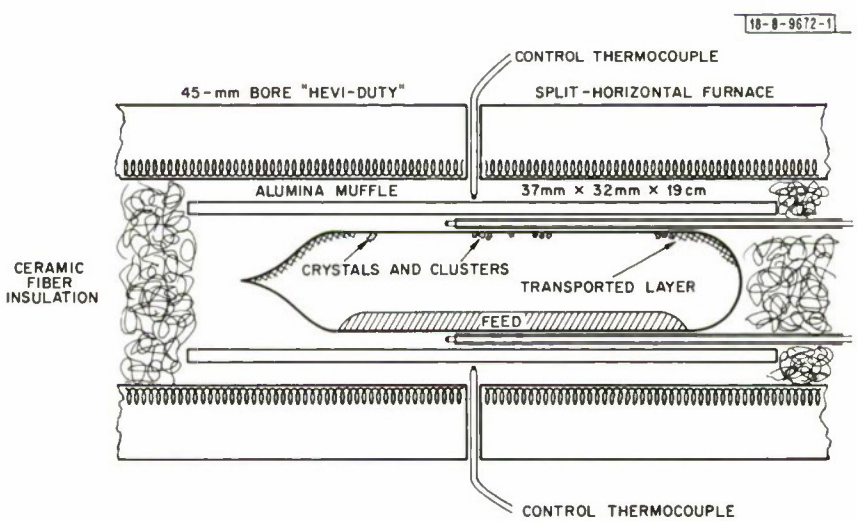

Fig. II-11. Apparotus for growth of $Fe_{1-x}Cu_xCr_2S_4$ single crystals by vapor transport.

Fig. II-12. Single crystals of $Fe_{1-x}Cu_xCr_2S_4$ grown by vopor tronsport.

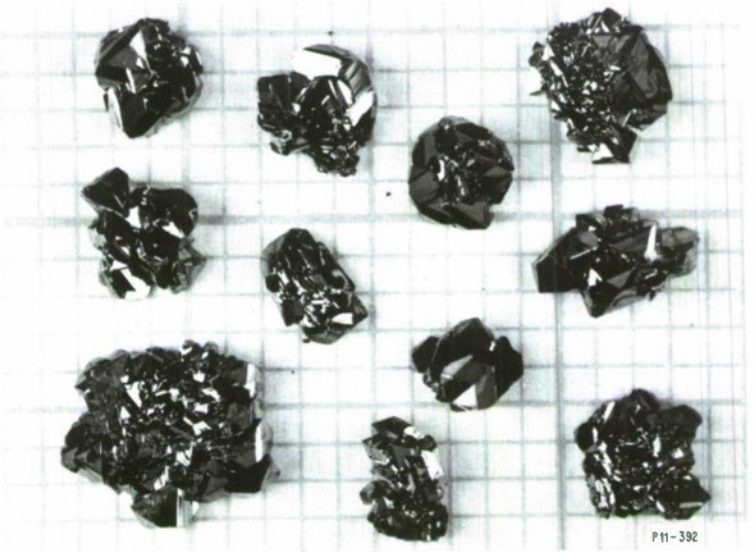

Fig. II-13. Clusters of $Fe_{1-x}Cu_xCr_2S_4$ crystols grown by vopor tronsport.

For runs in which more than one type of transported deposit was formed in significant amounts, a sample of each type was analyzed for Fe, Cu and Cr. The different types were found to have essentially the same Fe-Cu-Cr ratios except for runs in which more than about 75 percent of the feed was transported. The transported material contains somewhat more Fe and less Cu than the original feed powder. This change in composition indicates that the vapor transport process used in our experiments is more effective for Fe than for Cu. This is consistent with the observation that the overall rate of transport increased with increasing Fe content. The decrease in x for the transported alloys is 0.01 to 0.05. There is a corresponding increase in x for the untransported feed, which frequently is also enriched in Cr.

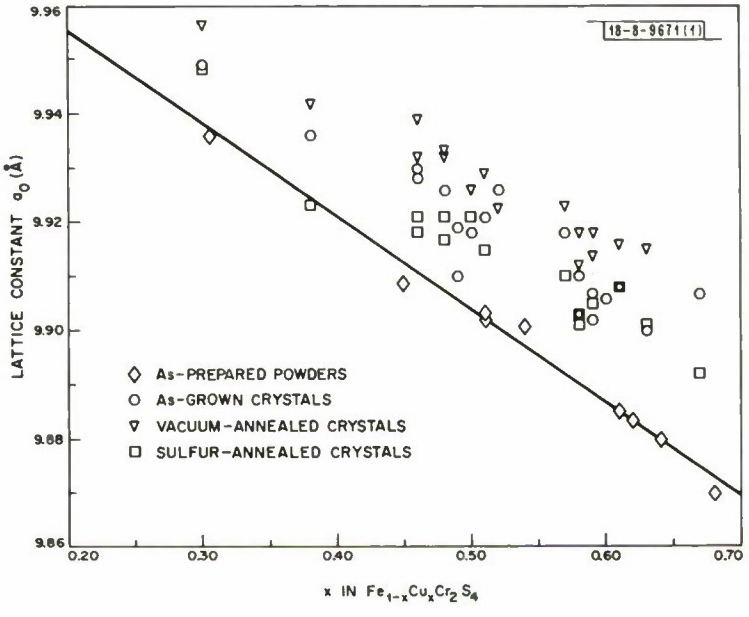

Fig. II-14. Lattice parameter (a_o) vs composition for $Fe_{1-x}Cu_xCr_2S_4$ alloys.

The lattice parameter (a_o) values which we have measured for $Fe_{1-x}Cu_xCr_2S_4$ samples are plotted in Fig. II-14 as a function of the x values obtained by chemical analysis. The data for as-prepared feed powders are in excellent agreement with the Vegard's law line drawn between the a_o values measured for $FeCr_2S_4$ (9.989 Å) and $CuCr_2S_4$ (9.819 Å). However the values of a_o for as-grown crystals (represented by circles) are 0.005 to 0.025 Å higher than those given by the Vegard's law line. Furthermore the a_o values differ by 0.005 to 0.010 Å for as-grown crystals with the same value of x. This variation shows that the lattice parameters of the transported crystals are significantly affected not only by the Fe-to-Cu ratio but also by some other variable, presumably the S-to-metal ratio, the Cr content, or both.

To investigate the effect of the S-to-metal ratio, we attempted to change this ratio by annealing vapor-grown crystals or clusters of crystals at 750° C for 4 to 100 hours in sealed ampules which had either been evacuated or loaded with sufficient S to establish the saturated vapor pressure. The a_o values measured after annealing are plotted in Fig. II-14. The changes in S-to-metal

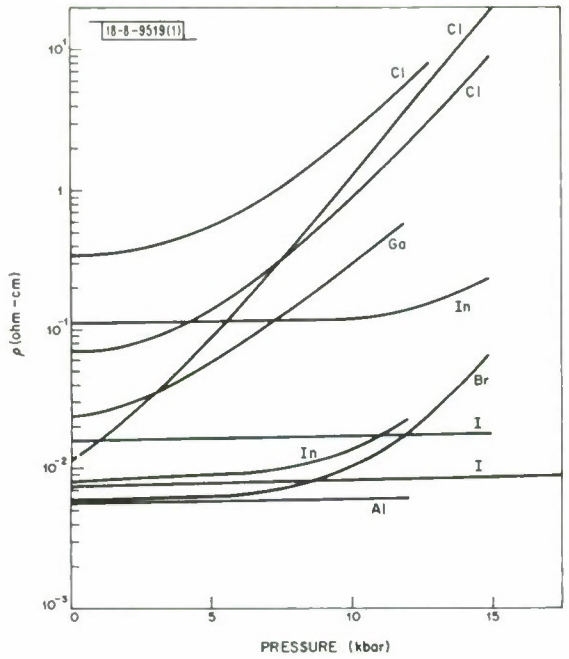

Fig. II-15. Room temperoture resistivity vs hydrostotic pressure for donor-doped n-type CdTe.

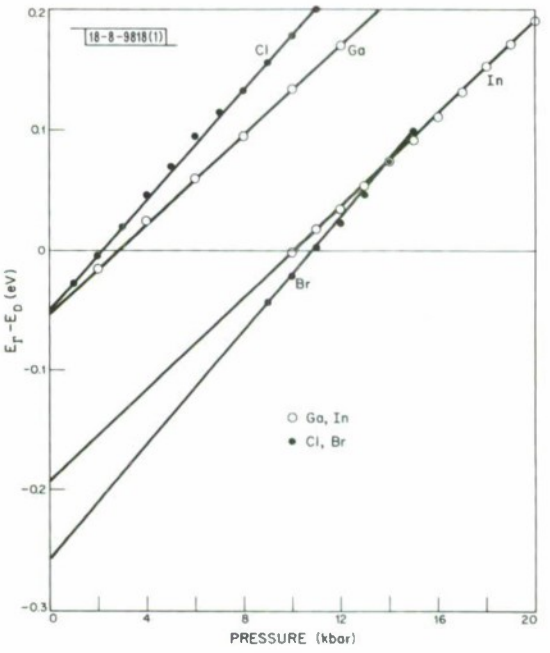

Fig. II-16. Donor energy level with reference to Γ conduction band minimum ($E_\Gamma - E_D$) os o function of hydrostotic pressure for CdTe.

ratio are sufficient to produce significant changes in a_o, which is reversibly increased by vacuum annealing and decreased by S annealing. Constant values of a_o were obtained by successive vacuum anneals after a total annealing time of 8 to 24 hours. These values can be fit fairly well by a straight line parallel to the Vegard's law line for the as-prepared powders but lying 0.025 Å higher. Presumably this line gives the a_o values for samples with compositions at the metal-rich limit of the homogeneity range for $Fe_{1-x}Cu_xCr_2S_4$. The lower line for the as-prepared powders presumably gives the a_o values for samples with compositions at the sulfur-rich limit of the homogeneity range. However, the a_o values for the transported crystals after sulfur annealing rarely reach this line.

M. D. Banus

E. NON-Γ DONOR LEVELS IN n-TYPE CdTe

The Group III elements Al, Ga and In and the Group VII elements Cl, Br and I are all effective donor impurities in CdTe. We have measured the effects of pressure and temperature on the resistivity and Hall coefficient of CdTe samples heavily doped with these elements. The resistivity values measured at room temperature are plotted on a logarithmic scale in Fig. II-15 as a function of hydrostatic pressure. Except for the samples containing Al and I, the resistivity increases markedly with increasing pressure. Hall coefficient measurements under pressure have shown that this increase in resistivity ρ is due almost entirely to a decrease in carrier concentration n, not to a decrease in mobility. The strongest effects are observed for the Cl-doped samples. Results in quantitative agreement with these have been reported by Foyt, Halsted and Paul[9] for nominally undoped samples of CdTe; we believe that these samples actually contained Cl.

Similar changes in carrier concentration with pressure have been observed for n-type samples of GaAs, GaSb and $GaAs_{1-x}P_x$ alloys.[10] They are generally attributed to the transfer of electrons from the lowest conduction band minimum at Γ into donor levels associated with higher minima, as these minima and therefore the donor levels are lowered relative to the Γ minimum by the application of pressure. Adopting this same explanation for the present results, we conclude that Cl, Br, Ga and In all introduce non-Γ donor levels into CdTe.

For each of these dopants, we have used the carrier concentrations measured in the pressure experiments to calculate the difference in energy between the donor level and the Γ minimum as a function of pressure. The differences are plotted as a function of pressure in Fig. II-16. For each impurity, the points can be very well represented by a straight line. The slopes of the four lines are similar, but those for Cl and Br are somewhat higher than those for Ga and In. Extrapolation of the lines to the ordinate gives the following values for the positions of the donor levels at atmospheric pressure: Ga, −0.05; Cl, −0.05; In, −0.19; and Br, −0.26 eV. The minus signs mean that each of the donor levels lies above the Γ minimum at atmospheric pressure.

No significant decrease in carrier concentration can be produced by pressure until the donor level is sufficiently close to the Fermi level. This suggests that we failed to observe pressure effects in samples doped with Al or I because these impurities introduce non-Γ levels located so far above the Γ minimum that the maximum pressure we used was too low to reduce the carrier concentration. Alternatively, the donor levels due to these impurities might be associated with the Γ minimum. There is no way to distinguish between these possibilities on the basis of our data.

In several cases the donor energy levels calculated from the room temperature data have been compared with ionization energies obtained by measuring the carrier concentration at various fixed pressures as a function of temperature. The results of these measurements on a Cl-doped sample are shown in Fig. II-17. At the two higher pressures, where the Cl donor level is below the Γ minimum, as the temperature is reduced below room temperature the carrier concentration initially decreases sharply as the electrons are transferred into the Cl levels. The ionization energies calculated from the data in this region are in good agreement with the values obtained from the room temperature measurements.

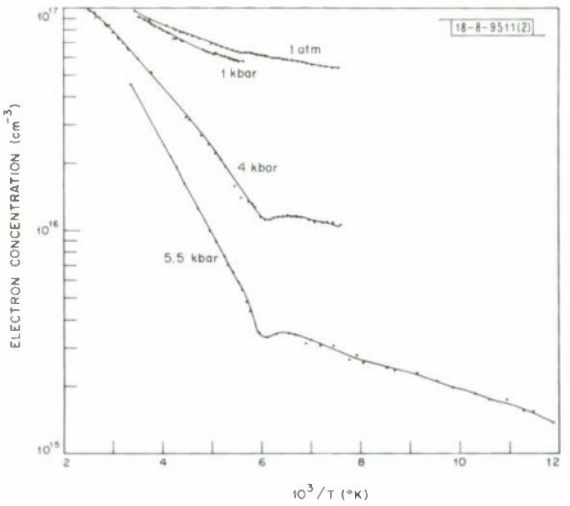

Fig. II-17. Carrier concentration vs reciprocal absolute temperature for Cl-doped CdTe at fixed hydrostatic pressures.

At about 160° to 170° K, the two higher pressure curves exhibit an abrupt decrease in slope. On the basis of our earlier study of S donors in GaSb,[11] we believed that this change in slope was probably due to a decrease in the rate of electron transfer sufficient to prevent equilibrium from being achieved between the conduction band and the Cl levels at low temperatures. This hypothesis was confirmed by two hysteresis experiments in which resistivity measurements were made as a function of temperature on a Cl-doped sample (1) cooled rapidly to 77° K at 4 kbar and then warmed slowly to room temperature at the same pressure, and (2) cooled rapidly to 77° K at 4 kbar and then warmed slowly to room temperature after the pressure had been reduced to 2 kbar.

Similar hysteresis phenomena have been observed in our pressure-temperature experiments on CdTe samples heavily doped with Br, Ga and In and also in transport and photoconductivity measurements on S-doped GaSb[11] and $GaAs_{1-x}P_x$.[12] In each of these cases, as well as in Cl-doped CdTe, the time constant for electron transfer between the donor levels and the Γ minimum increases strongly as the temperature decreases. Pressure experiments show that the donor levels are associated with higher conduction band minima. This correlation leads us to conclude that there is a causal relationship here – that is, the fact that electron transfer in these materials is a thermally activated process is a consequence of the fact that the donor levels involved are not associated with the Γ minimum.

G. W. Iseler
J. A. Kafalas
A. J. Strauss

REFERENCES

1. T.B. Reed, R.E. Fahey and A.J. Strauss, Solid State Research Report, Lincoln Laboratory, M.I.T. (1971:1), p. 18, Fig. II-2.
2. J.M. Longo, P.M. Raccah and J.B. Goodenough, Solid State Research Report, Lincoln Laboratory, M.I.T. (1966:3), p. 20, DDC AD-641498.
3. S. Geller, J. Chem. Phys. 24, 1236 (1956).
4. J.B. Goodenough and J.M. Longo, Landolt-Bornstein Tabellen Neu Serie III/4a (Springer-Verlag, Berlin, 1970), p. 126.
5. J.B. Goodenough, Czech. J. Phys. B17, 304 (1967), DDC AD-667872.
6. G. Haacke and L.C. Beegle, J. Phys. Chem. Solids 28, 1699 (1967).
7. _____, J. Appl. Phys. 39, 656 (1968).
8. H.L. Pinch, "Chemical Vapor Transport Growth of Some Chromium Chalcogenide Spinels," ACCG Conference on Crystal Growth, National Bureau of Standards, Gaithersburg, Md., 11-13 August 1969.
9. A.G. Foyt, R.E. Halsted and W. Paul, Phys. Rev. Letters 16, 55 (1966), DDC AD-635337.
10. W. Paul, Proceedings of Ninth International Conference on the Physics of Semiconductors, Moscow, 1968 (Nauka, Leningrad, 1968), Vol. 2, p. 16, and references therein.
11. G.W. Iseler and A.J. Strauss, Bull. Am. Phys. Soc. 12, 404 (1967).
12. M.G. Craford, G.E. Stillman, J.A. Rossi and N. Holonyak, Phys. Rev. 168, 867 (1968).

III. PHYSICS OF SOLIDS

A. ELECTRONIC BAND STRUCTURE

1. Spin Splitting in $Pb_{1-x}Sn_xSe$ from Shubnikov-de Haas Measurements†

In order to observe spin splitting, Shubnikov-de Haas measurements on $Pb_{1-x}Sn_xSe$ crystals have been extended to high magnetic fields. Both n- and p-type samples with compositions $x = 0.17$ and $x = 0.20$ have been studied. We obtain values of ν the ratio of spin splitting to Landau level separation ($\nu = m^*g/2m_o$) equal to either 0.65 or 1.35 for $x = 0.17$. To decide between these two values we note that data on magnetic field dependence of $Pb_{1-x}Sn_xSe$ laser diode emission[1] shows that the combined conduction and valence band spin splitting is greater than one for x greater than 0.15. Thus, in our case $\nu = 1.35$ is the correct choice for samples with $x = 0.17$ and either 2.2×10^{17} holes/cm^3 or 4.6×10^{17} electrons/cm^3. The results for this and other samples are shown in Table III-1.

Assuming mirror bands we have derived an expression for the g-factor of the carriers from existing theory.[2] From this, one can get a simple result for ν in terms of the effective mass m^* and the parameters m/m_t and g_ℓ, which include the effects of higher bands:[2] $\nu = (g_\ell/2 - m/m_t)\, m^*/m + E_g/|E_g|$. From previous fits of the theory to the experimental effective mass values, m/m_t was determined to be about 9.0. Using this and fitting ν to sample F we find that g_ℓ must be less than 1.0. If we take $g_\ell = 0$ and use the previously calculated values of m^*/m, which differ less than 10 percent from the experimental values shown in Table III-1, we obtain the calculated values of ν and g. (For these samples, which are beyond the band inversion point, E_g is negative.) The agreement with experiment is at least qualitative. In particular, the correct dependence of ν on carrier concentration seen in comparing samples C and D is predicted.

The Fermi surface of both holes and electrons appears to be nearly spherical for these samples, and the spin splitting also appears to be independent of orientation.

J. Melngailis
T. C. Harman
W. C. Kernan

2. Capacitance-Voltage Measurements on InAs and PbTe Schottky Barriers: Effects of the Inverted Surface

We have measured the dc voltage dependence of the incremental capacitance of evaporated metal Schottky barriers on p-InAs and p-PbTe. In order to interpret these results it was necessary to develop a theoretical treatment which properly accounted for the presence of the inverted surface in these barriers. Our theoretical results provide the correct interpretation of capacitance voltage data when the band bending in the semiconductor exceeds the energy gap. The experimental data on p-InAs at 4.2°K and low carrier concentration p-PbTe at 77°K are in agreement with this theoretical treatment when an arbitrarily large surface inversion is assumed. This result confirms our previous suggestion[3] that low work function metals (e.g., Pb, In, Sn)

† These experiments were carried out using the high field facilities of the Francis Bitter National Magnet Laboratory, M.I.T.

TABLE III-1

$Pb_{1-x}Sn_xSe$ g-FACTORS

Sample	x	Type and Carrier Concentration	Measured			Calculated	
			m^*/m_o	$\lvert\nu\rvert$	$g = 2\lvert\nu\rvert m_o/m^*$	$\lvert\nu\rvert$	$\lvert g\rvert$
Calawa, et al.[1]	0.22	Diode	0.036	1.3	72	1.32	73.6
F	0.17	$p = 2.2 \times 10^{17}$	0.030	1.3 ± 0.05 (or 0.7)	87	1.29	80.5
A	0.17	$n = 4.6 \times 10^{17}$	0.040	1.35 ± 0.07	68	1.36	68.0
B	0.17	$n = 6.0 \times 10^{17}$	0.044	1.35 ± 0.07	61	1.38	65.6
K	0.20	$p = 1.9 \times 10^{17}$		1.25 ± 0.07		1.35	69.3
C	0.20	$n = 2.0 \times 10^{17}$	0.035	1.22 ± 0.07	69	1.35	69.3
D	0.20	$n = 1.7 \times 10^{18}$	0.062	1.48 ± 0.07	48	1.54	51.3

produce strong surface inversion on p-PbTe and offers an alternate interpretation for the capacitance data by Meade and Spitzer[4] who first noted the presence of the inversion layer on p-InAs.

Theory:- Figure III-1(a) shows the contact potential diagram for the usual Schottky barrier where the barrier height $q\varphi_{bp}$ is less than the energy gap. In most semiconductors the Fermi level position at the surface is determined by surface states and lies between the band edges as illustrated here. For this contact potential, the charge in the semiconductor is primarily the negative charge of ionized acceptors in the depleted region and calculation of the capacitance is quite simple. The capacitance per unit C/A can be written in terms of N_A, the bulk carrier concentration, ϵ, the static dielectric constant, q, the electron charge, V, the applied voltage and V_I, the voltage intercept, as

$$(C/A)^{-2} = [2/qN_A\epsilon]\,(V_I - V) \quad , \tag{III-1}$$

$$V_I = \varphi_{bi} - 2/5\xi_B \quad \text{for} \quad q\xi_B >> kT,\ q\varphi_{bi} << E_g \quad . \tag{III-2}$$

The built-in potential φ_{bi} and the Fermi energy $q\xi_B$ are shown in Fig. III-1(a). In this case the capacitance-voltage characteristic is a simple means of determining the built-in potential φ_{bi}. Figure III-1(b) illustrates the contact potential when a degenerate inverted region is present.

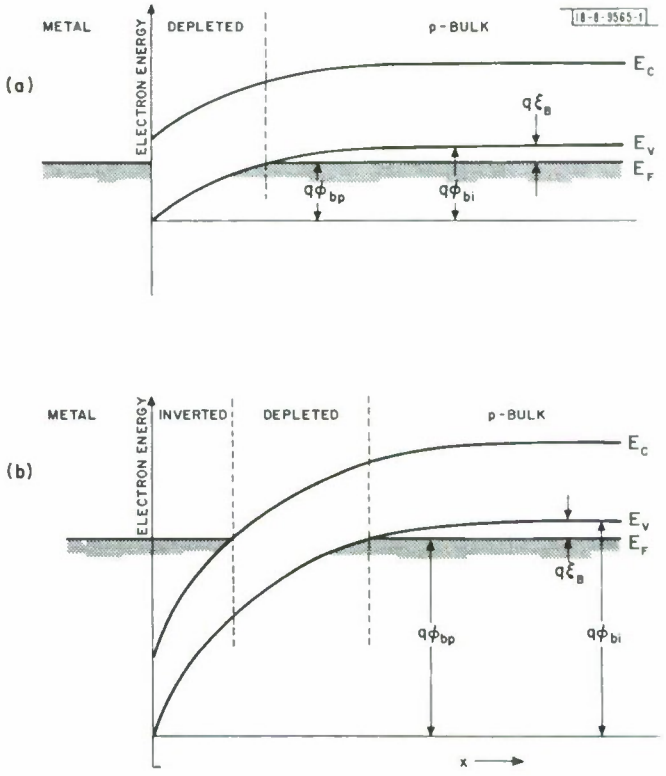

Fig. III-1. Barrier potential vs distance for a metal-semiconductor barrier illustrating (a) usual Schottky barrier and (b) inverted surface barrier.

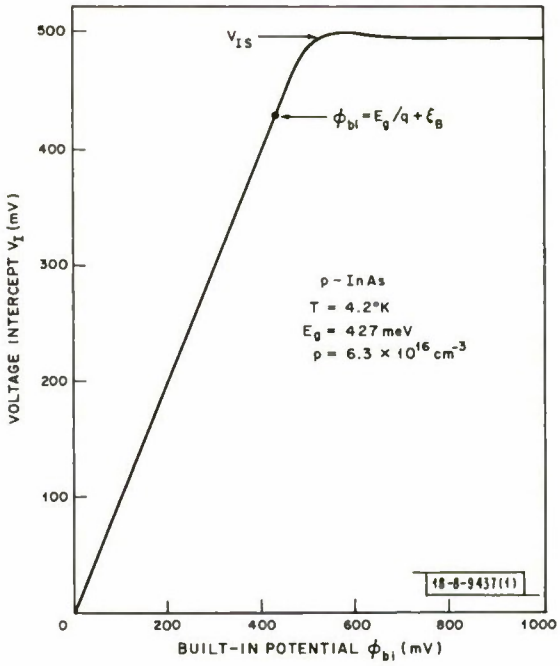

Fig. III-2. Calculated variation of the C^{-2}-V voltage intercept V_I with built-in potential for p-InAs illustrating saturation at V_{IS}.

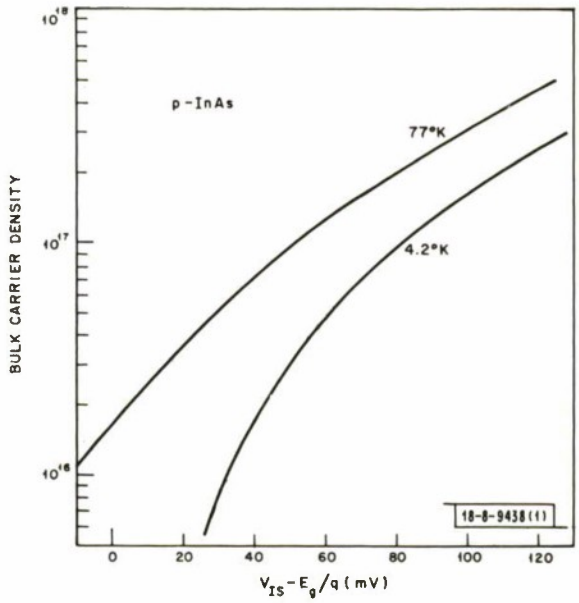

Fig. III-3. Calculated variation of the saturation voltage intercept V_{IS} with bulk carrier density for p-InAs at T = 77° and 4.2°K.

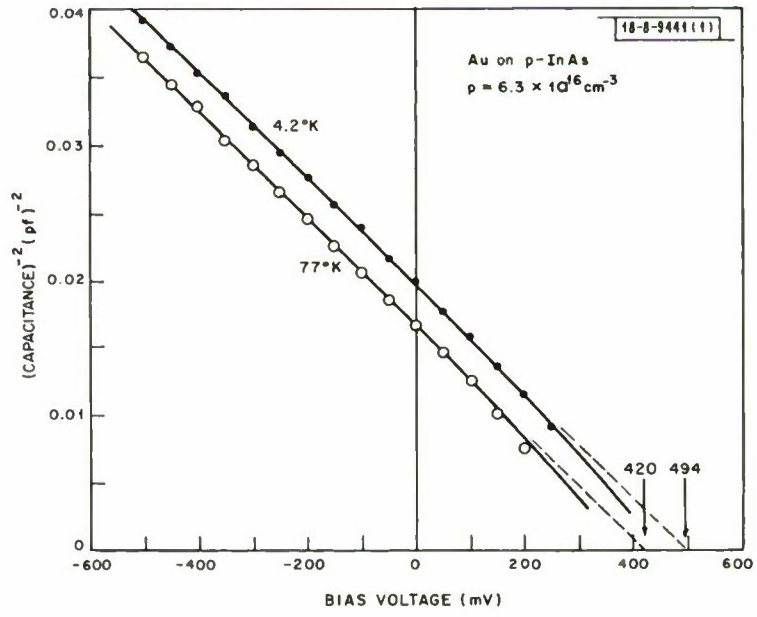

Fig. III-4. Experimental capacitance-voltage data on p-InAs at T = 77° and 4.2°K. Voltage intercepts of 420 and 494 mV are indicated by vertical arrows.

For this case, there are two components of the negative charge in the semiconductor: the ionized acceptor charge and the mobile electron charge in the conduction band. Calculation of the capacitance requires accounting for the components of the charge flowing in each electrode in response to a voltage change. The mobile charge in the inverted surface is supplied by the metal electrode and must be calculated self consistently with the potential variation by using Poisson's equation. For both InAs and PbTe it is necessary to use a two-band Kane model to describe the conduction band nonparabolicity. In our calculations we also included the effects of nonzero temperature. The general expression derived for Fig. III-1(b) is given by

$$(C/A)^{-2} = [2/qN_A\epsilon] \left\{ \frac{d}{d\varphi_B} \int_{\varphi_B}^{\varphi_s} [1 - p(\varphi, \varphi_B)/N_A] \times \left[\int_{\varphi_B}^{\varphi} \{1 - p(\varphi', \varphi_B)/N_A + n(\varphi')/N_A\} \, d\varphi' \right]^{-1/2} d\varphi \right\}^{-2} . \quad \text{(III-3)}$$

Equation (3) is an integral over potential with φ_B and φ_s being the value of the potential in the bulk and at the surface. For the cases we have studied this expression is approximately given by

$$(C/A)^{-2} = [2/qN_A\epsilon] (V_I - V) \quad \text{(III-4)}$$

which is identical to Eq. (III-1) except for the identification of V_I.

The voltage intercept V_I is no longer given by Eq. (III-2), but has the interesting dependence illustrated in Fig. III-2. In this figure the linear variation of V_I with φ_{bi} for small values is given by Eq. (III-2) and is the small barrier result valid for the usual Schottky barrier. The abrupt saturation of V_I at V_{IS} results from the presence of charge in the degenerate inverted surface region and is the significant new result of our theoretical treatment. It indicates that in this case for built-in potential more than 50 mV larger than $\varphi_{bi} = E_g/q + \xi_B$ there is no effect of the size of the built-in potential on the capacitance-voltage characteristic. It is interesting to note that while the voltage intercept V_I of Eq. (III-1) is nearly independent of the semiconductor properties (since, typically, $\xi_B << \varphi_{bi}$) the saturation value V_{IS} is a relatively strong function of bulk carrier concentration, band nonparabolicity and temperature. Increasing the density of states of the conduction band tends to reduce the saturation value toward the value at $\varphi_{bi} = E_g/q + \xi_B$, where charge first begins to enter the conduction band. The strong dependence of V_{IS} on carrier concentration is shown in Fig. III-3 for the same p-InAs parameters as Fig. III-2. For small barriers the dependence of the voltage intercept V_I is very slight, amounting to a few millivolts over the concentration range of $p = 10^{16}$ to 10^{18} cm^{-3}.

Experimental:– Experimental data taken on a gold p-InAs barrier at T = 4.2° and 77°K is shown in Fig. III-4. These data were taken using a 100 kHz capacitance bridge with the device immersed in liquid nitrogen or liquid helium. Samples were prepared by depositing gold barriers about 100 μm in diameter and 1000 Å thick on freshly etched ⟨100⟩ samples. Typical capacitance values were 5 to 10 pF. These data show the expected linear dependence of the inverse capacitance squared on voltage, Eq. (III-4), with a voltage intercept V_I of 494 mV. The solid lines through the experimental points are the calculated results of Eq. (III-3) using

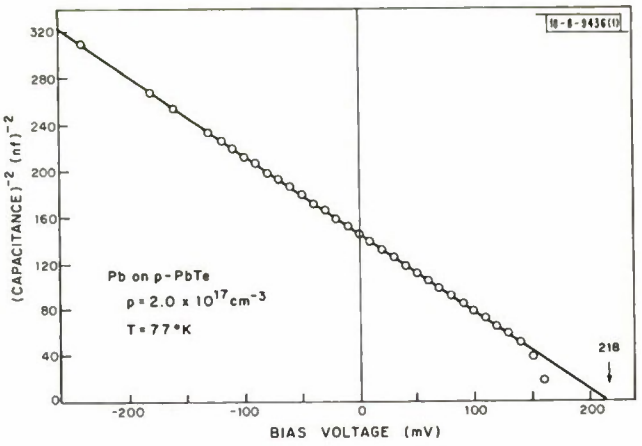

Fig. III-5. Experimental capacitance-voltage data an p-PbTe at T = 77°K. Valtage intercept af 218 mV is indicated by vertical arrow.

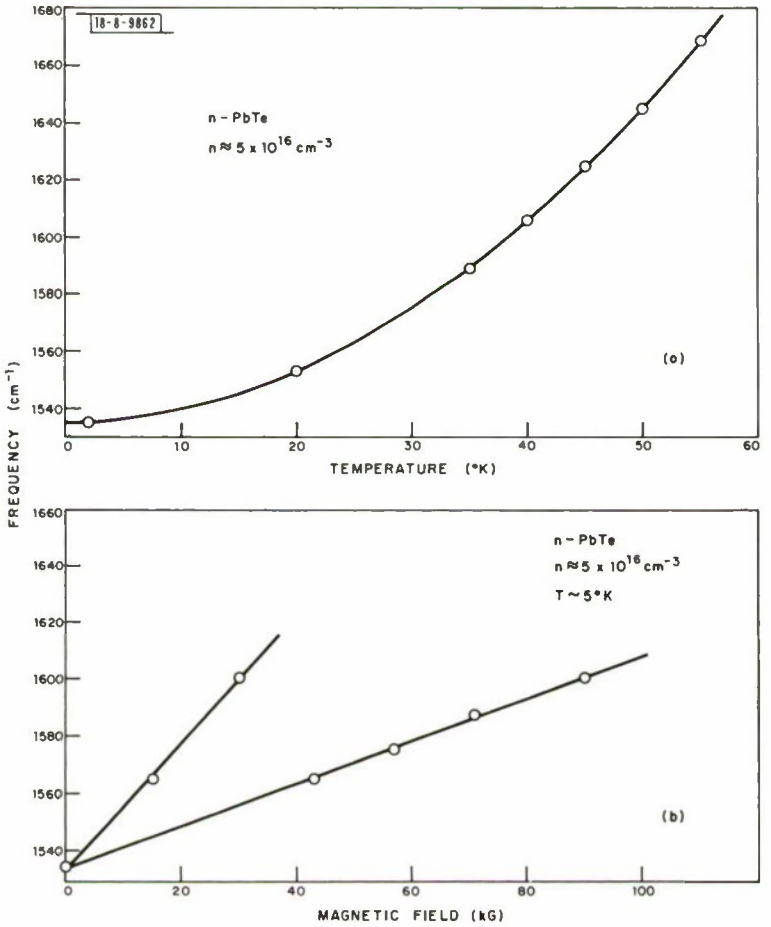

Fig. III-6. Tuning af aptically pumped PbTe stimulated emissian at the energy band gap as a functian af (a) temperature and (b) magnetic field (T ≈ 10°K).

E_g = 427 mV at T = 4.2°K. The inverted surface model accounts for most of the observed decrease in intercept between T = 4.2° and 77°K, but fitting the data at T = 77°K requires an energy gap about 15 mV less than the accepted value. We believe that this discrepancy can be explained by the presence of compensating donor and acceptor levels known to be present in p-InAs. However, we have no measure of their density and have not attempted to include them in the calculation. Figure III-5 shows similar data obtained on p-PbTe at T = 77°K using a 21 MHz bridge. This device was prepared by evaporating Pb on an air cleaved ⟨100⟩ sample. The calculated saturation voltage intercept V_{IS} is 215 mV, within a few mV of the observed intercept. The solid line is a straight line through the experimental points. These data and similar data on high concentration p-PbTe confirm our previous suggestion that a strongly inverted surface is produced by low work function metals on this semiconductor.

K. W. Nill
J. N. Walpole†

B. LASER SPECTROSCOPY, SCATTERING AND NONLINEAR EFFECTS

1. Stimulated Emission from Optically Pumped PbTe

We have made some preliminary studies of optically pumped stimulated emission (6.0 to 6.5 μ) from homogeneous n-PbTe platelets (nominal 0.5 × 0.5 × 0.25 mm) using a discretely tunable (5.2 to 6.5 μ) liquid nitrogen-cooled carbon monoxide gas laser as the pump. The sample faces were all cleaved (100) planes. The CO laser was Q-switched yielding a peak power of 100 to 200 W with a pulse width of about 200 nsec at a 100 Hz repetition rate. The pump radiation was focused on the broad face of the samples with a 10 cm focal length BaF_2 lens. Figure III-6(a) shows the quasi-continuous tuning of one of the lasers ($n_e \sim 5 \times 10^{16}$ cm^{-3}) as a function of temperature. The data were taken with the sample in a variable temperature optical dewar with the temperature controlled to within 0.1°K. The stimulated emission occurred in several longitudinal cavity modes and the data points shown locate the approximate center of these modes. Stimulated emission was obtained between 1.8° and 55°K. The pump wavelength was 5.84 μ. Figure III-6(b) shows the tuning of a similar sample ($n_e \approx 5.0 \times 10^{16}$ cm^{-3}, $\mu \approx 35{,}000$ cm^2/volt-sec at 77°K) as a function of magnetic field. The sample was placed on a cold finger in a continuous flow liquid helium dewar in a superconducting magnet. The magnetic field was directed along the (100) axis of the sample. Conversion efficiencies in these preliminary experiments were low with an upper bound of 1 percent.

The pumping of PbTe with the CO laser holds two promising possibilities which are under investigation: (1) resonant bulk pumping near the energy band gap to achieve high efficiency lasers; and, (2) stimulated spin-flip scattering from the conduction electrons. High quantum efficiencies have been reported for resonantly pumped GaAs[5] and longitudinally pumped InSb with inversion in the bulk due to carrier diffusion.[6] Low threshold, high efficiency stimulated spin-flip scattering has been observed in resonantly pumped InSb using a CO laser.[7] The close match between the PbTe energy gap and the CO laser output is favorable for efficient conversion between the pump radiation and the stimulated photoluminescence as well as strong resonant enhancement of the spin-flip scattering. High quality, low carrier concentration (for small free

† Department of Electrical Engineering, M.I.T.

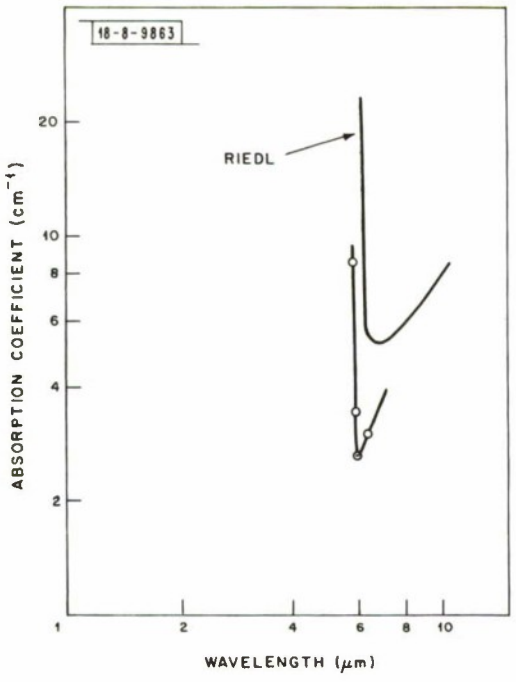

Fig. III-7. Optical absorption coefficient of n-PbTe near the absorption edge at 77°K.

carrier losses) material is essential for both of these phenomena. The optical absorption coefficient of a typical sample ($n_e \approx 1.4 \times 10^{17}\,cm^{-3}$, $\mu \approx 35{,}000\,cm^2/volt\text{-}sec$) at 77°K is shown in Fig. III-7 and compared with data of Riedl[8] for a sample with $n_e \approx 3.9 \times 10^{17}\,cm^{-3}$. The minimum absorption coefficient of less than $3\,cm^{-1}$ at $6\,\mu$ is encouraging.

K. W. Nill
F. A. Blum

2. Raman Scattering and Infrared Absorption in FeF_2

The Raman scattering study of an intense line at $1082\,cm^{-1}$ in FeF_2 has been augmented by infrared absorption measurements and Raman scattering measurements of MnF_2 and MgF_2 doped with Fe^{2+}.

In the infrared absorption measurements we have confirmed the presence of the $1115\,cm^{-1}$ line reported by Stout, et al.[9] with selection rule H || c. In addition we see a somewhat weaker line at $1082\,cm^{-1}$ (the same energy as the Raman excitation, within the experimental accuracy), having the same linewidth, $\sim 30\,cm^{-1}$, as the Raman line, and with selection rule H $\perp$ c. Measurements were performed at 300°, 77° and 5°K, with this absorption being seen only at 5°K.

Raman scattering measurements in samples of MnF_2 doped with up to 0.8 percent (atomic) Fe^{2+} and MgF_2 doped with ~0.5 and 1 percent Fe^{2+} revealed no excitations apart from the phonons. The previous measurements on FeF_2 in a magnetic field with 180° scattering geometry were repeated in a 90° scattering configuration, with no apparent differences. In both cases, magnetic fields up to 80 kG had no visible effect on the Raman spectrum.

The present experimental evidence suggests that this unknown excitation at $1082\,cm^{-1}$ is either a pair-excitation involving a crystal field state and magnon, or a single ion excitation

involving the exchange field and spin-orbit coupling in an as yet unknown manner. Further theoretical work is continuing on this question.

S. R. Chinn

3. Two-Magnon Raman Scattering in Two-Dimensional Antiferromagnets

Preliminary calculations are underway to extend the finite temperature, two-magnon scattering theory discussed in a previous report, to a study of simple two-dimensional antiferromagnetic systems, e.g., K_2NiF_4. Many properties of the two-dimensional systems depend critically on the long wavelength magnon spectrum. Without anisotropy, there can be no long range order (for $T > 0$) in the two-dimensional case.[10] This is essentially due to a divergence in the number of long wavelength magnons in the absence of anisotropy. In contrast to this, two-magnon Raman scattering measures primarily the short wavelength (zone edge) magnon spectrum and is expected to be insensitive to details of anisotropy. Furthermore, we expect the present Hartree-Fock theory to provide information about the short range order of the system, up to temperatures well above the critical temperature for long range order.

R. W. Davies
S. R. Chinn
H. J. Zeiger

4. Permanent Photo-Dielectric Lens Effect in CdS

A laser-induced lens has been observed in bulk samples of high-conductivity single crystal CdS at temperatures above 100°C. The development time for lens formation is a function of the laser power and wavelength as well as the crystal temperature. The highest sensitivity appears to be near the He-Ne laser wavelength, 6328 Å. On cooling the crystal after development, the lens is fixed; on heating above 275°C, the lens may be erased. Its permanence at room temperature is at least three days. The refractive index change is negative leading to a defocusing of the beam. No anisotropy of the effect is observed for various light polarization or propagation directions in the crystal; the lens itself is radially symmetric. High-resistivity, sulfur-compensated crystals do not show the effect.

Several earlier observations of photo-dielectric effects in CdS[11,12] and other solids[13-15] have been reported. A variety of models[11-16] have been advanced to explain these results, but none apply to the unique characteristics arising in the present study.

The simple experimental arrangement is illustrated in Fig. III-8. A laser beam is focused by a positive 10-cm lens on or near a thick CdS sample mounted on a heater and the far-field pattern is observed. With no crystal the TEM_{oo} Gaussian mode is obtained. Then with the crystal placed in the positions of the second lens, the lower patterns are observed, illustrating that the refractive index change is negative. An induced positive lens would reverse the lower two patterns. The ring structure, emphasized by overexposure, results from the spherical aberrations of a Gaussian-profile lens as discussed by Whinnery, et al.[17] The patterns shown are for a nominally pure, $2 \times 2 \times 1$ cm, high-conductivity ($\sigma \sim 0.1$ mho/cm) crystal grown by Harshaw and illuminated with 6328 Å light. A similar high-conductivity $1 \times 1 \times 1$ cm crystal from Crysteco also shows the effect. On the other hand, $1 \times 1 \times 1$ cm sulfur-compensated high-resistivity crystals from Harshaw and Crysteco show no beam distortion. All the crystal faces are optically polished flat to within $\lambda/2$.

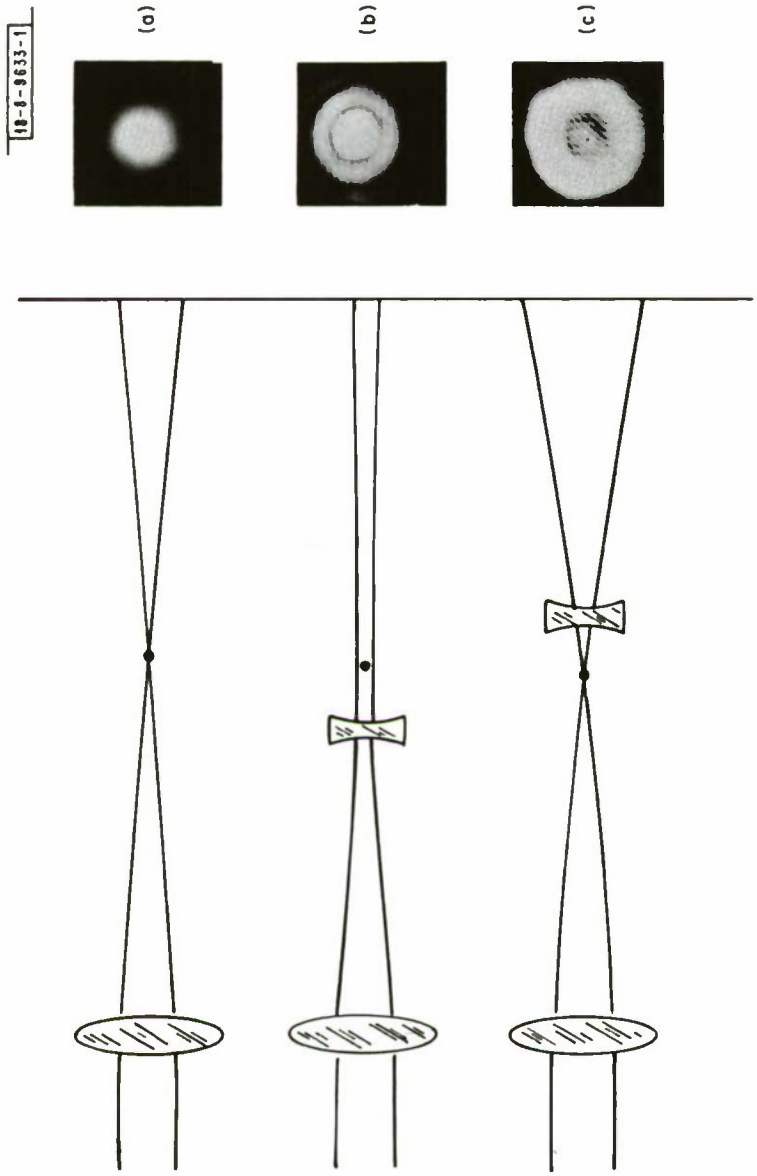

Fig. III-8. Far-field patterns from laser-induced negative lens in CdS. The sample position is indicated by the double concave lens.

The characteristic time to develop the lens is given in Fig. III-9 as a function of temperature for various laser powers at 6328 Å. This development time, τ_D, is somewhat difficult to define uniformly for all laser powers; but it is arbitrarily taken as when the first ring of Fig. III-8(b) is sharply formed – not when a steady state is reached. Dynamically this ring may collapse into the central spot, being replaced sequentially by higher order rings. The number of rings that develop and contract before saturation increases with increasing laser power. However, the definition of τ_D is chosen to indicate a fixed refractive index change or "exposure."

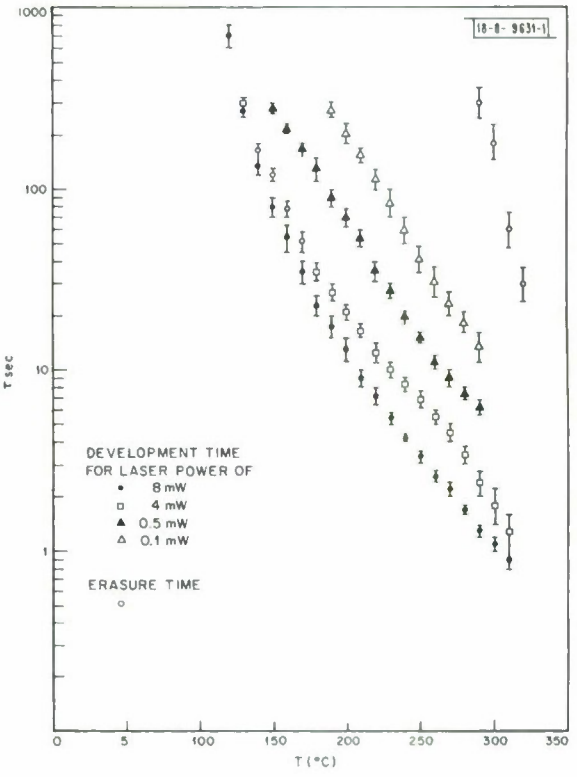

Fig. III-9. Lens development and erasure times in CdS for 6328 Å.

The erasure time, τ_E, at high temperatures is measured after saturated development of the lens with the 8 mW laser beam. A weak probe is obtained by suddenly attenuating the beam by a factor of 1000.

The sensitivity of the effect to the yellow and red krypton laser lines is considerably lower. At 196°C the development time for 110 mW at 5682 Å is about 40 sec and for 200 mW at 6471 Å is about 10 sec. It should be noted that at these temperatures, the yellow light is absorbed quite strongly (~75 percent) because the band gap decreases with temperature. In the red, however, the maximum absorption is ~20 percent for the 2 cm path length at the highest temperatures reached. Applications of this effect to holography[18] and bulk storage and to dielectric waveguides[14] have been demonstrated in other materials. The sensitivity of CdS to He-Ne radiation is rather high in this regard, but a limited spectral response and a relatively poor optical quality are drawbacks. The defects and striations in presently available crystals give a large amount of scatter and probably limit the spatial resolution.

K. B. Kanarek†
C. D. Wyche
A. S. Pine

† Department of Electrical Engineering, M.I.T.

REFERENCES

1. A. R. Calawa, J. O. Dimmock, T. C. Harman and I. Melngailis, Phys. Rev. Letters 23, 7 (1969), DDC AD-694137.
2. J. O. Dimmock, Proceedings of the Conference on the Physics of Semimetals and Narrow Gap Semiconductors (Dallas, 1970); J. Phys. Chem. Solids Suppl. (to be published).
3. K. W. Nill, A. R. Calawa, T. C. Harman and J. N. Walpole, Appl. Phys. Letters 16, 375 (1970), DDC AD-706308.
4. C. A. Meade and W. C. Spitzer, Phys. Rev. Letters 11, 358 (1963).
5. N. G. Basov, A. Z. Grasiuk, V. F. Efimkov, I. G. Zubarev, V. A. Katulin and J. M. Popov, J. Phys. Soc. Japan (Supplement) 21, 277 (1966).
6. R. J. Phelan, Solid State Research Report, Lincoln Laboratory, M. I. T. (1965:2), p. 1.
7. A. Mooradian, S. R. J. Brueck and F. A. Blum, Appl. Phys. Letters 17, 481 (1970); S. R. J. Brueck and A. Mooradian, Appl. Phys. Letters 18, 229 (1971).
8. H. R. Riedl, Phys. Rev. 127, 162 (1962).
9. J. W. Stout, M. I. Steinfeld and M. Yuzuri, J. Appl. Phys. 34, 1141 (1968).
10. N. D. Mermin and H. Wagner, Phys. Rev. Letters 17, 1133 (1966).
11. W. C. Wang and P. Das, Appl. Phys. Letters 12, 204 (1968); 13, 331 (1968).
12. A. Ashkin, B. Tell and J. M. Dziedzic, IEEE J. Quant. Elect. 3, 400 (1967).
13. A. Ashkin, G. D. Boyd, J. M. Dziedzic, R. G. Smith, A. A. Ballman, J. J. Levinstein and K. Nassau, Appl. Phys. Letters 9, 72 (1966).
14. W. J. Tomlinson, I. P. Kaminow, E. A. Chandross, R. L. Fork and W. T. Silfvast, Appl. Phys. Letters 16, 486 (1970).
15. F. S. Chen, J. Appl. Phys. 40, 3389 (1969).
16. G. Thomas and B. L. Sopori, J. Appl. Phys. 41, 603 (1970).
17. J. R. Whinnery, D. T. Miller and F. Dabby, IEEE J. Quant. Elect. 3, 382 (1967).
18. F. S. Chen, J. T. LaMacchia and D. B. Fraser, Appl. Phys. Letters 13, 223 (1968).

IV. MICROELECTRONICS

A. THIN FILM PROGRAM ON BEAM-LEADED SUBSTRATES

Dielectrically-coated, flexible-metal, beam-leaded substrates are being implemented using organic and inorganic dielectric coatings on several different metal foils. The inorganic, dielectric-metal foil system that has shown the most promise is SiO_2 sputtered on 0.002 inch molybdenum foil. The optimum fabrication cycle to fabricate beam-leaded substrates on these molybdenum foil pieces using two levels of metallization with beam-leaded crossovers is as follows.

(1) Clean the molybdenum foil in detergent, rinse and etch lightly in 20:1 H_2O:HF.

(2) Sputter approximately 3 micrometers (30,000 Å) of SiO_2 onto the foil. The sputtering is done using a fused quartz target in an RF system with a pure argon atmosphere. During sputtering the foil is isolated both thermally and electrically from the anode by floating the substrate on a piece of glass. This procedure insures a uniform heating of the foil substrate without having to resort to substrate heaters and elaborate means of achieving good thermal contact between the substrate and the anode.

(3) Sputter a duplex layer of molybdenum and gold on top of the SiO_2, plate the gold to 0.0005 inch and photolithographically form the interconnection and beam-lead pattern minus the crossovers.

(4) Coat the circuit side of the substrate with KTFR and photolithographically form the chip apertures by etching through the SiO_2 and the molybdenum foil, while protecting the back side of the substrate. The chip apertures could be etched easily from the back side if a simple means of aligning the chip aperture mask from front to back were available.

The circuit is now complete except for forming the second layer of metallization in the form of beam-leaded crossovers. The following procedures are necessary only if two layers of metal are required.

(1) Strip the substrate of all resist and sputter a duplex layer of titanium and copper over the entire circuit side of the substrate.

(2) Plate the copper to approximately 0.001 inch and flash about 10 microinches of gold on top of the copper.

(3) Spray coat the substrate with Shipley AZ 1350H positive acting photoresist, expose holes in the resist for the vias through the copper to the interconnect metallization and etch through the gold flash and the copper/titanium.

(4) Re-expose the resist to define the crossovers and plate approximately 0.0003 inch of gold from via to via. Strip the resist and etch away the gold flash, the copper and the titanium underlayer.

The beam-leaded substrate is now complete and ready for chip mounting and beam-lead bonding.

The organic dielectric being used exclusively at this time is a polyimide, which is used as a photosensitive (selectively soluble) solution of polyamic acid in N-methyl-2-pyrollidone sensitized by adding a saturated solution of potassium dichromate in dimethyl sulfoxide.* This

* R. E. Kerwin and M. R. Goldrick, "Thermally Stable Photoresist," Polymer Engineering and Science (to be published).

dielectric has been used with great success on magnesium foil with aluminum interconnections. Work is currently under way to enable aluminum interconnections to be formed on polyimide-coated copper substrates. The process that is being used to form aluminum interconnections and beam leads on the magnesium and copper substrates is as follows.

(1) Polyamic acid solution is spin-coated on the foil substrates to a thickness of one micrometer (10,000 Å). The resist is then exposed and developed leaving chip apertures. Then the polyamic acid is imidized by heating at 300°C for 30 minutes. This process is repeated to give a polyimide coating of 20,000 Å total thickness.

(2) The substrate has 60,000 to 100,000 Å of aluminum evaporated over the polyimide, and the aluminum is formed photolithographically into the interconnection pattern using a hot, phosphoric acid based etchant. Then the chip apertures are etched in the foil using the polyimide as a mask and cold chromic acid as the chemical milling agent. The cold chromic acid does not attack the aluminum but will etch both magnesium and copper.

(3) The resist is removed and the substrate is complete with a single level of metallization. A second level of metal can be easily achieved using the polyimide photoresist as an organic dielectric between layers of metal. Aluminum beam-leaded crossovers are also a possibility.

Although considerable success has been achieved etching the foils from the front, etching from the back side would be an improvement. Work is under way to develop an alignment procedure that would protect the circuit from the front and etch the foil from the back. Another problem that has been encountered when using copper foil is lack of adhesion of the polyimide to the foil, resulting in undercutting and dielectric lifting during etching processes. This difficulty is attributed to oxidation of the copper during the imidization process. Work is under way to evaluate a procedure for imidizing in nitrogen instead of air, as is done now.

F. J. Bachner

B. GENERAL SEMICONDUCTOR WORK

Several examples of major programs that are primarily semiconductor oriented are described to indicate the general nature of the semiconductor effort.

(1) TRAPATT Diodes:– Recent fabrication has resulted in diodes that exhibit the desired electrical specifications. The physical size of the diodes is 5 mils with a C_o = 4 pfs, and BV_R = 90 V. The thermal resistance has been improved over earlier diodes. Test results are not available as yet but previous runs with earlier diodes resulted in low efficiency diodes that oscillated in the TRAPATT mode at X-band.

(2) GaAs Mixer Diodes:– Various resistivity and epilayer thickness materials have been used to fabricate 2 to 3 μ gold Schottky barrier diodes. The process has been improved by utilizing only ⟨100⟩ oriented material, etching rather than lapping back contacts and reducing the thickness of the wafer from 5 to 3 mils. This has lowered the series resistance and increased the yield and quality of die separation. Good noise figures have been obtained in mixer operation at 55 GHz. Further processing is continuing in order to optimize material specifications and processing variables, such as back contact characteristics, plating, oxide dielectric, etc.

(3) E-Birds:– The latest results on planar P-diffused N-type silicon E-Birds indicate stable operation with good efficiency at a peak power level of 0.5 kW with a low duty cycle. The experimental electron beam shield on the device has worked out well and withstands the electron beam without degrading the P-N junction. A new package design has been devised to incorporate a more practical shield and also to allow much greater heat dissipation. N-diffused P-type silicon E-Birds have been fabricated and are at the final packaging step.

(4) LSI:– Custom processing continues utilizing the boron and phosphorus deposition and diffusion equipment. Recent processing has produced betas of 90 to 100, BV_{CBO} of 140 V, BV_{CEO} of 60 V and BV_{EBO} of 7 V.

(5) Nuclear Radiation Particle Detector:– An array of devices has been successfully fabricated to determine the suitability of the over-all fabrication procedure. Changes in the basic material and geometry are under way to lower the present 500 to 700 diode voltage breakdown.

(6) Diode Matrix:– The 10 × 10 diode matrix for read only memory applications has been completed and is in testing. Individual diodes have 60 V_R and satisfactory forward characteristics.

An epitaxial reactor for N-type silicon epitaxial growth and for the deposition of Si_3N_4 has been received and is presently being installed in the Class 10,000 clean room. This will enable us to continue work on the SIMTOP process for the several programs which utilize mesa structures and for the development program on monolithic planar-mesa integrated circuits.

R. A. Cohen

C. MASK GENERATION

In the past quarter, efforts to reduce long term problems in the area of paper tape generation on the 360 computer system have progressed to the point where individual users of the mask generation programs no longer need worry about the actual paper tapes. The Mannplot program has been modified to automatically store all paper tape data on a special account assigned to Group 87. Group 87 personnel perform actual paper tape generation using new programs developed for the purpose. Comparison of these paper tapes with the source data is then performed and bookkeeping is automatically handled by another set of programs, with the result that bad paper tapes no longer reach the mask facility, and record keeping is improved and simplified.

Plans to eliminate paper tape entirely from the system are still under consideration.

The mask facility itself continues to improve as techniques are refined and new equipment added. A new contact printer is on order along with several other significant additions; and, the physical area in which the equipment is located will again be expanded and upgraded in the coming months.

N. B. Childs

D. BONDING, PACKAGING AND ENVIRONMENTAL TESTING

Bonding:– IMPATT diodes are now being packaged and bonded by techniques which provide improved heat-sinking characteristics. The improvement in the ease of assembly provided by this package contributes to an improved over-all yield, while also providing good protection for the bonds.

Packaging:– A package design for the multielement particle detector is being developed. A 40 lead DIP package will permit fabrication of the 20 beam leads as well as the 20 wire bonds to a special substrate which has been designed for this device.

Process Control:– Process control and inspection procedures have been instituted to monitor our assembly techniques. Variations in bonding procedures are evaluated, for instance, by means of pull tests on sample bonds and scanning electron microscope examinations of critical areas. Inspection and test results are correlated to processing procedures. These control procedures are being further developed to provide a mechanism for effective quality control.

T. F. Clough

DOCUMENT CONTROL DATA – R&D

(Security classification of title, body of abstract and indexing annotation must be entered when the overall report is classified)

1. ORIGINATING ACTIVITY *(Corporate author)* Lincoln Laboratory, M.I.T.	2a. REPORT SECURITY CLASSIFICATION Unclassified 2b. GROUP None

3. REPORT TITLE

Solid State Research

4. DESCRIPTIVE NOTES *(Type of report and inclusive dates)*

Quarterly Technical Summary for 1 February through 30 April 1971

5. AUTHOR(S) *(Last name, first name, initial)*

McWhorter, Alan L.

6. REPORT DATE	7a. TOTAL NO. OF PAGES	7b. NO. OF REFS
15 May 1971	64	44

8a. CONTRACT OR GRANT NO. F19628-70-C-0230 b. PROJECT NO. 649L c. d.	9a. ORIGINATOR'S REPORT NUMBER(S) Solid State Research (1971:2) 9b. OTHER REPORT NO(S) *(Any other numbers that may be assigned this report)* ESD-TR-71-145

10. AVAILABILITY/LIMITATION NOTICES

Approved for public release; distribution unlimited.

11. SUPPLEMENTARY NOTES	12. SPONSORING MILITARY ACTIVITY
None	Air Force Systems Command, USAF

13. ABSTRACT

This report covers in detail the solid state research work of the Solid State Division at Lincoln Laboratory for the period 1 February through 30 April 1971. The topics covered are Solid State Device Research, Materials Research, Physics of Solids and Microelectronics. The Microsound work is sponsored by ABMDA and is reported under that program.

14. KEY WORDS

solid state devices
materials research
crystal growth
magnetism
electronic band structure
proton bombardment
laser scattering
infrared
Raman scattering
magneto-optical research
microelectronics